DEGREE PROJECT IN ENGINEERING PHYSICS,
SECOND CYCLE, 30 CREDITS
STOCKHOLM, SWEDEN 2020

Facile Microwave Assisted Aqueous Chemical Synthesis of Bi_2Te_3 and Sb_2Te_3 Thermoelectric Materials

An approach towards green chemistry for sustainable chemical reduction synthesis

MOON PAUL

KTH ROYAL INSTITUTE OF TECHNOLOGY
SCHOOL OF ENGINEERING SCIENCES

Facile Microwave Assisted Aqueous Chemical Synthesis of Bi_2Te_3 and Sb_2Te_3 Thermoelectric Materials

An approach towards green chemistry for sustainable chemical reduction synthesis

MOON PAUL

Master Thesis
Engineering Physics
Stockholm, Sweden 2020

KTH Royal Institute of Technology
Department of Applied Physics
SE-106-91, Stockholm, Sweden

TRITA-SCI-GRU 2020:009

Supervisor: Bejan Hamawandi

Examiner: Muhammet Toprak

KTH Royal Institute of Technology
Department of Applied Physics
SE-106-91, Stockholm, Sweden

Abstract

Thermoelectric (TE) materials are capable of interconverting between heat and electrical energy. They can be used to harvest low and high-grade waste-heat effectively, and are all solid-state materials without any moving parts, which gives them a high operational reliability. Nanostructuring is important in the field of TEs due to the resultant low thermal conductivity originating from enhanced phonon scattering. Generally, TE materials are synthesized through highly energetic techniques, needing high temperatures and prolonged reaction durations. Green synthesis of TE nanoparticles is desired to overcome the environmental challenges imparted using conventional synthesis methods. A facile green chemical synthesis method has been developed for producing low dimensional TE nanomaterials. Bi_2Te_3 and Sb_2Te_3 hexagonal nanoplatelets have been synthesized using reduction reaction. Non-hazardous and commonly available precursors, and water as the solvent have been used instead of harmful organic ones. Microwave assisted rapid heating, as a very effective volume heating, was used for the synthesis of highly crystalline Bi_2Te_3 and Sb_2Te_3, significantly reducing the reaction time of synthesis, with a high yield of conversion. The reaction mixture was heated in the microwave reactor for only 2 minutes at 220°C. The effect of pH in the reaction mixture, as well as optimal reaction conditions have been studied. Scanning electron microscopy (SEM) and X-ray powder diffraction (XRD) have been used to study the morphology and crystal structure of as-synthesized TE materials. Dynamic light scattering (DLS) – zeta potential analysis has been used to study the particle size distribution and surface charge. An attempt has also been made to scale-up the synthesis process for Bi_2Te_3. The optimized aqueous synthesis method for Bi_2Te_3 and Sb_2Te_3 nanomaterials and their characterization results are presented in detail.

Moon Paul

Keywords: Microwave synthesis, Bi_2Te_3, Sb_2Te_3, thermoelectric materials, hexagonal plates, green synthesis

Contents

List of Abbreviations and Symbols

DOS	Density of States
DLS	Dynamic Light Scattering
ICs	Integrated Chips
nm	Nanometre
QDs	Quantum Dots
RT	Room Temperature
SEM	Scanning Electron Microscope
TE	Thermoelectric
XRD	X-ray Diffraction
0D	Zero Dimensional
1D	One Dimensional
2D	Two Dimensional
3D	Three Dimensional
k_B	Boltzmann's Constant
I	Current
E_g	Energy Bandgap
η	Efficiency
ρ	Electrical Resistivity
σ	Electrical Conductivity
k_e	Electronic Thermal Conductivity
k_l	Lattice Thermal Conductivity
μ	Mobility
$\prod$	Peltier Coefficient
S	Seebeck Coefficient
V_s	Seebeck Voltage
ΔT	Temperature Difference
$\frac{dT}{dx}$	Temperature Gradient
k	Thermal Conductivity
ΔV	Voltage Difference
zT	Thermoelectric Figure of Merit

List of Figures

List of Tables

Tools and Softwares used

HighScore Plus	Crystallography analysis
ImageJ	Size analysis
Milestone flexiWAVE	Microwave synthesis
Origin 85	Plotting graphs
Philips PANalytical X'Pert Pro Powder Diffractometer	XRD measurement
SEM FEG column and a 30 kV FIB column	SEM images
Malvern Zetasizer Nano ZS90	Zeta potential and size distribution
Zetasizer	Zeta potential and size distribution

Acknowledgements

This master thesis has been a great learning experience for me. I acknowledge the contribution of each and every single person who has been a part of this journey.

First and foremost, I would express my gratitude to Prof. Muhammet Toprak, for allowing me to join the thermoelectrics group and work on this project. He has been extremely supportive and patient with me and every interaction with him has taught me something new. I would like to take this opportunity to express my sincere gratitude to my supervisor, Mr. Bejan Hamawandi. He deserves all the appreciation for guiding me throughout the course of the project. He has been a mentor and a friend to me, and it has always been easy to explore new ideas with him. I have never had a dull conversation or interaction with both of them. It is indeed my pleasure to have Prof. Muhammet and Bejan as my mentors. I would also like to express my gratitude to the other members of the BIOX group, especially Hazal Batili, Carmen Vogt, Rabia Akan and Yuyang Li, for being wonderful lab mates and providing me a helping hand whenever required. They have made sure time spent in the lab was informative, safe and productive. I would also like to thank Gianmarco Saladino for his inputs. I would also like to extend my appreciation to the Department of Applied Physics in AlbaNova for their support in the completion of this project.

I am grateful to my friends for their encouragement and being my family away from home. Last but not the least I would like to thank my family. I am forever indebted to my parents and siblings for their unconditional support and motivation.

Moon Paul

(intentionally left blank)

Chapter 1

Introduction

We are facing a global energy crisis due to our huge dependence on non-renewable sources and as the consumption of these sources has increased, the likelihood of their availability for a long term has diminished. The burning of fossil fuels and the emission of greenhouse gases, like carbon dioxide, methane, has reached an alarming level. In 2019, the Earth Overshoot Day has been reported on July 29. This marks the date in a year when humanity's demand for ecological resources exceeds what the Earth can regenerate for that given year. This information has been published by *Global Footprint Network*, an international sustainability organization that has pioneered the Ecological Footprint. It has also been mentioned that 29th July 2019 has been the earliest date for the Earth Overshoot Day, and it has moved up two months over the past 20 years [1]. In order to meet the future challenges of energy and climate change, it is paramount for emerging technologies to develop revolutionary, renewable, and sustainable solutions.

This thesis will provide an overview on the recent advances on thermoelectric nanomaterials and the various synthesis methods. A bottom-up aqueous chemical synthesis route using microwaves is studied to produce scalable highly crystalline low dimensional nanostructures. This thesis intends to engage in the conversation for green nanotechnology.

1.1.Nanotechnology and Nanomaterials

Michael Faraday is viewed as one of the first researchers in nanoscience and nanotechnology when he had accidently made metallic gold colloids. In his diary dated 2 April 1856, Faraday had mentioned that while he was investigating the thin gold film under light, he had observed that the yellow and golden colour of the solution turned into a ruby colour [2]. He had described the metal particles in the dispersion of colloidal gold as *"very minute in their dimensions"* [3]. This can be recognized as the earliest nano-sized objects as the ruby colour is characteristic of gold nanoparticles [4]. Richard P. Feynman had given a visionary talk on December 29, 1959 at the annual meeting of the American Physical Society at the California Institute of Technology (Caltech) titled '*There is Plenty of Room at the Bottom*' [5]. It was then that the foundation of nanotechnology had been laid and the possibilities of exploring a revolutionary field had been provided.

Nanoscience refers to the science of study of the manipulation and control of materials operating on the nanoscale. Nanotechnology is defined as the design, characterization, production and application of structures, devices, and systems by controlling shape and size at the nanoscale [6]. Materials or objects having dimensions of the order of 100 nm or less are considered to be in the nanoscale [7]. The properties of materials at the nanoscale change significantly from their bulk materials. Properties of materials are size-dependent in this scale range. The materials at the nanoscale are made up of particles that have larger surface area as compared to the volume of the material. This suggests that as the surface area to volume ratio increases, the radius of the particle decreases and vice versa. This is due to quantum size confinement which affects the behaviour and properties of particles at the nanoscale [7]. Thus, at

the nanoscale, properties such as melting point, electrical conductivity, optical absorption, optical excitation and emission, photoluminescence, magnetic permeability, and chemical reactivity change as a function of the size of the particle and are hence are different from the bulk materials [8].

When a material shows a distinct change of electronic or optical properties due to the confinement in at least one dimension, it is referred to as a quantum-confined structure [9]. Nanomaterials are classified based on the number of degrees of freedom of the charge carriers in the three direction (dimensionality). When charge carriers are confined in three dimensions, *i.e.* zero degree of freedom, the nanomaterials are called zero-dimensional (0D) materials, like quantum dots (QDs). Similarly, nanostructures confined in two dimensions are referred to as one-dimensional (1D) materials, like quantum wires, nanorods, nanotubes, and nanostructures confined in one dimension are referred to as two-dimensional (2D) materials, like quantum wells and thin films. The large size crystals, with nano building blocks are the ones and zero confinement are known as 3D bulk structures [10].

The unique properties of matter that are observed at the nanoscale impart a wide spectra of applications in the areas of medicine, surgery, information technologies, energy production, conversion and storage, construction, manufacturing, electronics and instrumentation, environment, communication, material science, space exploration and security to many few [8, 10].

A major challenge of nanotechnology is to garner the benefits without causing risk to living beings and the environment [11]. Thus, it is of prime importance to identify, monitor and detect the toxicity of nanoparticles and its impact on the environment [11-12]. Vaseashta, A. *et al.* have investigated the role of nanomaterials to generate energy in order to reduce environmental pollution by incorporating the principles of green chemistry in the manufacture of nanomaterials [12]. Green chemistry is defined as the design of chemical processes and products to reduce or eliminate the use and generation of hazardous substances across all the life-cycle stages that have been shown to be economically profitable [13]. The staff of the U.S. Environmental Protection Agency (EPA) Office of Pollution Prevention and Toxins first coined the phrase *"Green Chemistry*" and started this initiative of productive collaboration between government, industry, and academia. Researchers went on further to define Green nanotechnology as the use of clean technology to enhance the environmental sustainability by the replacement of the existing hazardous products and use of green nano products that are more environmentally friendly throughout their lifecycle [14].

1.2.Thermoelectrics - Concepts and Research Advancement

Climeon, a Swedish product company working in generating clean electricity from low temperature systems, published a report on June 2019 stating that more than 50% of the energy used in the world today is wasted as heat [15]. The issue of an efficient waste heat recovery in transportation, housing and industrial sector and dissipation of energy in the form of heat in microelectronics has been recognised as a potential threat for managing the energy need of the world [16-17]. The exponential increase of the leakage current in transistors with temperature also poses a challenge in the ICs design [18]. Over the past few decades, due to the promising high efficiency of converting waste heat into electric energy, thermoelectric materials have attracted increasing attention in both the energy and environmental sectors [19]. Thermoelectric (TE) materials can directly convert heat into electricity and vice versa. TE devices have currently attracted huge interest because of their potential applications in energy harvesting, waste heat recovery in industries and transportation systems, chip cooling, solar cells, temperature sensing, military and space exploration [19-23, 34]. TE devices can be effectively used to harvest low- and high-grade waste heat. The advantages of TE generators are solid-state direct interconversion, no moving parts, noise free, compact structure, reliable and scalable. These make them ideal for small and distributed power generation [23-24]. However, the cost of thermoelectrics and their limitation in performance serves as a drawback for TE generators [24].

1.2.1 Thermoelectric Effects

When a material is subjected to a temperature difference across its ends, heat spontaneously flows from a region of higher temperature to a region of lower temperature. This flow of heat maintained until thermal equilibrium is reached and the temperature gradient vanishes. When a temperature gradient is applied to a thermoelectric material, the charge carriers (electron and holes) diffuse across a hot source to a cold source of the material [25]. In n-type materials, the electrons diffuse from one side of the junction to the other, whereas, in p-type materials, the holes diffuse from one side of the junction to the other, upon exposure to a temperature gradient. Figure 1 is a schematic thermoelectric device consisting of n-type and p-type thermoelectric elements wired electrically in series and thermally in parallel made up of thermoelectric couples. The schematic of the n-type and p-type thermocouple are also shown in Figure 1.

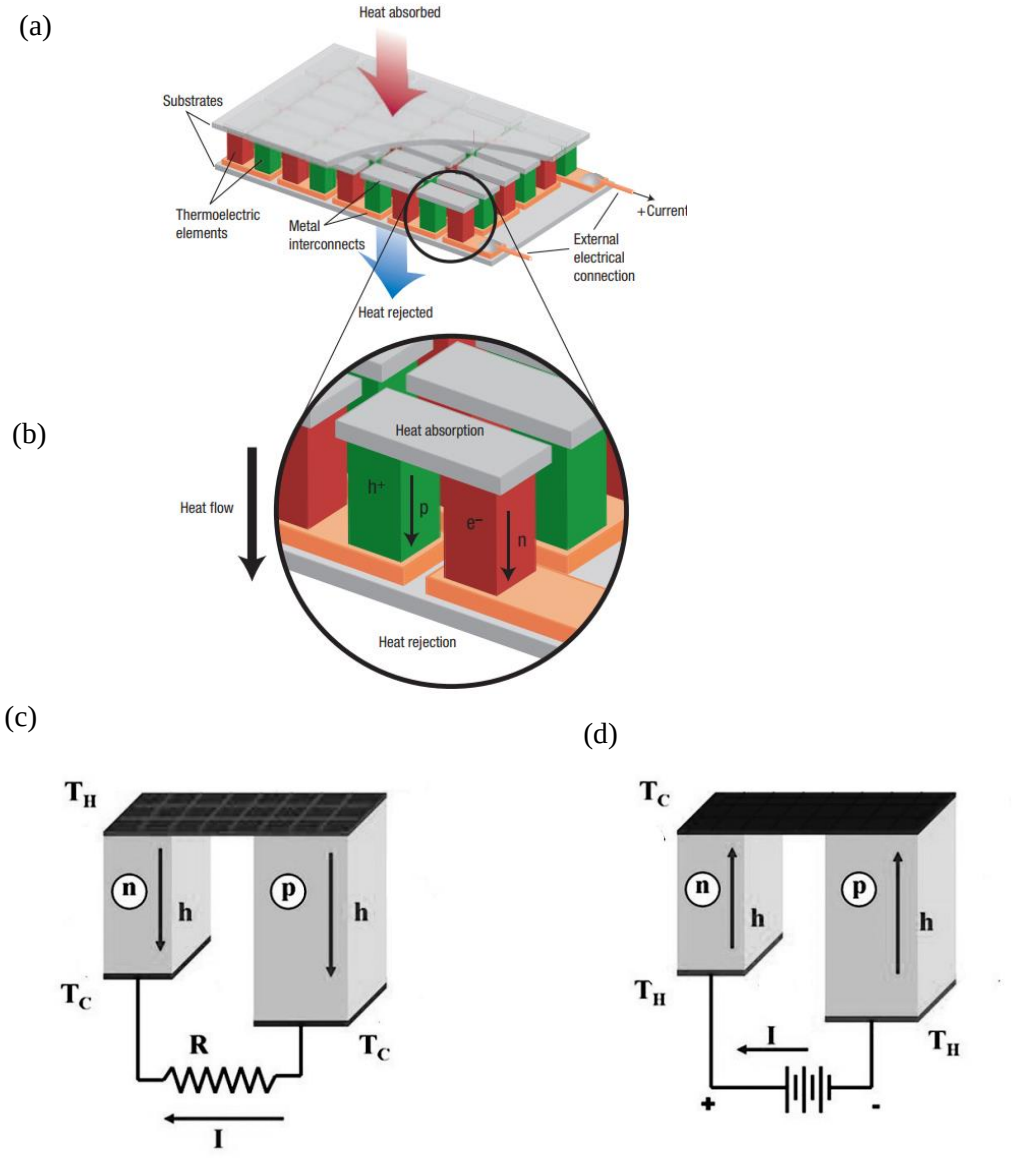

Figure 1. TE module showing the direction of charge flow on (a) cooling and (b) power generation. Basic schematic of n-type/p-type thermocouple in (c) TE cooler and (d) TE generator [24-25].

- ***Seebeck effect***

In 1821, Thomas Johann Seebeck had observed that if two dissimilar conducting materials were joined together and the junctions were maintained at different temperatures *(T and T+T')*, then an electric current flowed across the closed circuit. This is observed because there is a voltage difference across the circuit which is proportional to the temperature difference *(∆T)* [26]. The conversion of thermal energy to electrical energy in the form of electric current across junctions is given by the *Seebeck effect*. The *Seebeck voltage* (V_s) gives the magnitude of the *Seebeck effect*. The ratio of the voltage developed to the temperature difference is related to an intrinsic property of the materials and is termed as the *Seebeck coefficient (S)*, or the thermopower [27].

$$S = \frac{\Delta V}{\Delta T} \qquad \text{….. Equation 1}$$

The *Seebeck coefficient (S)* is denoted by a negative value ($S < 0$) for n-type semiconductors where the majority charge carriers are electrons and they diffuse from hot end to the cold end and by a positive value ($S > 0$) for p-type semiconductors where the majority charge carriers are holes which diffuse from hot end to the cold end [27]. The energy dependence of the conductivity is primarily determined by the density of states (DOS) and the *Seebeck coefficient* is proportional to the DOS [28].

- ***Peltier effect***

In 1834, Jean Charles Athanase Peltier had observed a heating or cooling effect when voltage is applied across two dissimilar conducting materials causing electric current to flow through the junctions. This causes heat to be removed from one junction and cooling is observed [29]. There occurs a temperature difference at the junctions and is called the *Peltier effect.* The Peltier heat is given by the heat absorbed (ΔQ) which is directly proportional to the current *(I)*, duration of current applied (Δt) and Peltier coefficient ($\prod$) [25].

$$\Delta Q = \prod I\, \Delta t \qquad \text{….. Equation 2}$$

In 1838, Friedrich Emil Lenz had illustrated the Peltier effect on a bismuth antimony junction. He placed a drop of water at the interface of two materials. When an electric current passed through the junction in one direction, the water froze, and consequently when the current was reversed, the ice melted into water [30]. Thus, he demonstrated that when current flows through a conducting circuit, heat is either absorbed or generated.

- ***Thomson effect***

William Thomson had observed that when a TE circuit is closed, the temperature gradient will cause the flow of electric current due to *Seebeck effect*, this flow of current will in turn given rise to Peltier heat which will be either absorbed or released from the one junction to the other due to the *Peltier effect* [31]. For this reason, *Peltier effect* is considered as the back-action counterpart to the *Seebeck effect* [32]. The *Thomson effect* is given by the relation of the absorption of heat *(Q)* across a homogeneous conductor due to the passage of current *(I)* and the temperature gradient (*dT/dx*).

$$Q = rI\,\frac{dT}{dx} \qquad \text{….. Equation 3}$$

Where *r* is known as the Thomson coefficient.

1.2.2. Microscopic Transport

At the microscopic levels, the TE effects can be attributed by considering the movement of the charge carriers – electrons and holes inside the solid structure. The basic requirements for a good TE device are given as follows: [33]

- Low thermal conductivity to reduce the parasitic heat losses which affects the overall efficiency of the device.
- High electrical conductivity to enhance the flow of the charge carriers.

- ***Electrical conductivity***

Electrical conductivity (σ) is the reciprocal of resistivity and electrical resistivity (ρ) is defined as the ratio of the electric field (E) to the current density at that point (j).

$$\sigma = \frac{1}{\rho} = \frac{e^2 n\tau}{m} = ne\mu \quad \text{….. Equation 4}$$

where, μ is the mobility of the charge carriers. Mobility is directly proportional to the electrical conductivity. In case of semiconductors, the charge carriers should be excited enough to cross the energy bandgap for conduction.

When the two ends of the conducting materials are maintained at a constant temperature, there is no net change in charge at both ends as the rate of diffusion is constant across the two ends. Due to scattering effects, the rate of diffusion at the hot and cold ends are different as these are energy dependent. This creates a higher density of carriers at one end of the material, resulting in splitting of positive and negative charges across the junctions. This gives rise to an electric field and a potential difference, Seebeck voltage *(V_s)* is generated. The electric field opposes the uneven scattering of carriers till an equilibrium is reached. Thus, by maintaining an increase in the temperature difference between the two ends, charges are generated which leads to an increase in the TE voltage, given as the equation 1 [33]. This is the property that is explored in TE materials and in order to achieve high electrical conductivity, high mobility of the electrons and small energy band gap of the conducting material are required. In case of semiconductors, the charge carriers should be excited enough to cross the energy bandgap for conduction. The electrical conductivity is thus given as,

$$\sigma \approx \sigma_o \exp\left[-\frac{E_g}{2k_B T}\right] \quad \text{….. Equation 5}$$

- ***Thermal conductivity***

In a crystal lattice, the collective oscillations of atoms are characterized by phonons. Phonons have energy (*hω)* and momentum and thus can conduct heat. When the phonons are arranged according to their energy value, the vibrational DOS can be obtained. The thermal conductivity can be related to the transfer of heat which arises due to the motion of the electrons *(k_e)* and the phonons in the crystal lattice *(k_l)* [34]. The phonon contribution to the specific heat at constant volume is given as:

$$k_l = \frac{1}{3} c_v v l \quad \text{….. Equation 6}$$

Where, c_v is the specific heat per unit volume, l is the phonon mean free path. Thus, minimum thermal conductivity can be achieved when the phonon mean free path is limited.

In a solid, the diffusion of charge carriers due to a thermal gradient can result in scattering processes with the phonons, thereby the phonons exchange energy and momentum with the electrons. These interactions are called electron-phonon interactions, which results in extra Peltier current due to the contribution of both the electrons and phonons, given as: [33]

$$\prod_j = (\prod_e + \prod_l)j \quad \text{….. Equation 7}$$

The Seebeck coefficient is expressed as the sum of the two contributions – electrons and phonons, given as a function of temperature expressed in equation 8 [25].

$$S\,(T) = S_e(T) + S_l(T) \quad \text{…. Equation 8}$$

The magnitude of S_l is dependent more on the relative strength of the scattering due to electron-phonon interactions, compared to the other phonon scattering (phonon - phonon and phonon–defects interactions). Since heat transfer is dominated by the charge carriers and electron–phonon interactions, is it important to maintain the phonon scattering [34]. Thus, in order to reduce thermal conductivity, increased phonon scattering is required.

1.2.3. Thermoelectric Efficiency

In 1911, Edmund Altenkirch had derived the efficiency of the thermoelectric devices by stating the different features required for a good thermoelectric material [35]. Later, Abram F. Ioffe had formulated a dimensionless quantity, *z*, which is now known as the most important characteristic of thermoelectric materials, is used to calculate the efficiency of thermoelectric devices. Thus, *zT*, called the figure of merit, is used determine the maximum efficiency of the energy conversion process (whether generating power or cooling) in the material [33].

Let us consider the pair of semiconductors with the n-type and p-type connected electrically in series and thermally in parallel in Figure 1. When one end is heated, a temperature gradient is created between the two sides which causes the charge carriers to diffuse from the hot side to the cold side. The Seebeck voltage is generated because of the diffusion of the carriers and an electric current flows across the closed circuit.

The efficiency of the system *(η)* is given as the ratio of the output power, (*P*) to the rate of the heat drawn from the source *(Q)*, so, $\eta = \frac{P}{Q}$

The current, *I*, is given in terms of the Seebeck coefficient, *S*, as: [36]

$$I = \frac{(S_p - S_n)(T_h - T_c)}{R_L + R_p + R_n} \quad \text{….. Equation 9}$$

Where, R_L, R_p, R_n is the resistance of the load, p-type material, and n-type material, respectively. S_p *and* S_n are the Seebeck coefficient of the p-type and n-type, respectively.

The output power given by the load resistor is given by: [36]

$$P = \left(\frac{(S_p - S_n)(T_h - T_c)}{R_L + R_p + R_n}\right)^2 R_L \quad \text{….. Equation 10}$$

The heat drawn from the source, *Q*, is given as: [36]

$$Q = (S_p - S_n)IT_h + (k_p + k_n)(T_h - T_c) \quad \text{..... Equation 11}$$

Where $k_p and\ k_n$ are the thermal conductances of the p-type and n-type TE material.

Thus, the efficiency is given in equation 12 as: [37]

$$\eta = \frac{T_h - T_c}{T_h} \frac{\sqrt{1 + zT_{avg}} - 1}{\sqrt{1 + zT_{avg} + \frac{T_c}{T_h}}} \quad \text{..... Equation 12}$$

where, T_{avg} is the average of T_c and T_h and the dimensionless figure of merit, *zT* is given in equation 13 expressed as: [35]

$$zT = \frac{S^2\sigma}{k}T \quad \text{..... Equation 13}$$

From the equation 13, it can be seen that if *zT* is much higher than unity, the model approaches the Carnot efficiency given as $\frac{(T_h - T_c)}{T_h}$ [36].

Since, *zT* is the measurement for the efficiency of TE materials, higher *zT* means higher efficiency of the TE device. The requirements for obtaining improved *zT* are thus summarized below:

- higher electrical conductivity, σ
- larger Seebeck coefficient, *S*
- lower thermal conductivity, k.

It has also been reported that the figure of merit, *zT* can be improved using nanostructures. The DOS near the Fermi level energy of the nanostructures can be enhanced by quantum confinement and this in turn will increase the Seebeck coefficient, and make this parameter separate from the electrical conductivity of the material. In nanostructures, the phonon mean free path is shorter than the electrons mean free path, and since there is a large density of interface, the phonons scatter more effectively and preferentially than electrons. This reduces the lattice thermal conductivity while not affecting the mobility and electrical conductivity. The enhanced *zT* of TE materials has been predicted or experimentally demonstrated for quantum dot and thin film superlattices, nanowires, nanotubes, and nanosheets [21, 38].

Kim H. S. *et al.* had considered the conventional efficiency formula to be unreliable as it is seen that the performance of these materials reduces over time due to aging. They have defined an engineering dimensionless figure of merit $(ZT)_{eng}$ and an engineering power factor $(PF)_{eng}$ as functions of the temperature difference between the cold and hot sides to accurately predict the practical conversion efficiency and output power, respectively [39].

The efficiency of a TE device is determined by the materials used in making the device, and thus the current focus of research is on finding better materials that can show improved TE properties.

1.3. Thermoelectric Materials

TE devices are predominantly composed of n-type and p-type materials where the majority charge carriers are electrons and holes respectively. Since the 1950s, the TE properties of narrow band gap semiconductors have been studied. Wood C. had studied the effect of optimum doping concentrations and the reduction of thermal conductivity by solid-solution doping. He had found that Bi_2Te_3, PbTe alloy and SiGe thermoelectric generators operated at room temperature to about 250-300°C, 600°C and 1000°C respectively and had z$T \approx 1$, also bismuth telluride had the highest zT of the three materials [40]. Over the years, comprehensive research has been done to discover good thermoelectric materials with high efficiency in order to commercialize them and that can show high zT at the required operating temperature. The most common materials were skutterudites, telluride-based materials (PbTe, Bi_2Te_3, Sb_2Te_3 etc.), rare earth chalcogenides ($La_{3-x}Te_4$, etc.), copper ion materials (Cu_2Se), SiGe alloys, ZnSb alloys, half-Heusler alloys, and clathrates [24, 38, 40-41]. Before the 1990s, the investigation for good TE materials was mainly limited to bulk materials. The TE properties of low dimensional structures started to attract attention from the early 1990s. Nanostructures had gained attention due to their low dimensionality which attributed to improved thermoelectric performance by the reduction of lattice thermal conductivity. Rowe *et al*. had studied the fine-grained polycrystalline Si-Ge alloys and reported a reduction in thermal conductivity with decreased grain size. This was due to the phonon scattering at the grain boundaries [42]. In 1993, Hicks and Dresselhaus theoretically showed that using low-dimensional structures could significantly improve the thermoelectric performance by the enhancement of the zT due to the quantum confinement effect of the low-dimensional structures [43-44].

Over the years, low-dimensional nanostructures have shown to reduce the lattice thermal conductivity due to the phonon blocking effect [45-48]. It has been observed that the most studied low-dimensional materials for low temperature applications (RT – 400K) has been Bi_2Te_3, Sb_2Te_3, $Bi_{0.5}Sb_{1.5}Te_3$, $Bi_2Te_{2.8}Se_{0.2}$ and for high temperatures (>900K) has been n-type PbSe-PbS, $Yb_{14}MnSb$, $Ca_3Ba_{0.05}Co_4O_{9+\delta}$ [38, 40-41]. Forman C. *et al*. had reported that 63% of the waste heat generated is at temperatures below 100°C [49]. Thus, in order to tackle this problem, it is important to synthesize materials that will serve as an effective thermoelectric material at room temperature. The two most common n-type and p-type thermoelectric materials for room temperature operations are Bi_2Te_3 and Sb_2Te_3 respectively and for this thesis these two materials have been considered. The thermoelectric materials near room temperature have the applications in sensing, energy harvesting, wearable thermoelectric and modules to power mobile devices [19].

1.3.1. Bismuth Telluride - Bi_2Te_3

The TE properties of Bi_2Te_3 were discovered in the early 1950s and since then they have become an important part in the thermoelectric industry known for their improved zT for low temperature applications. Bi_2Te_3 is a narrow indirect bandgap semiconductor that has a rhombohedral tetradymite-type crystal structure with the space group R-3m [50]. Bi is slightly less electronegative compared to more electronegative Te and in Bi_2Te_3 the valence of Bi is +3 (s2p0) and Te is −2. The chemical bonding between bismuth and tellurium atoms is mainly covalent with a small ionic contribution whereas it is a weak van der Waals attraction between the neighbouring Te layers. Figure 2. shows the structure of Bi_2Te_3 layers and it can be seen that the Te unit cell is composed of five covalently bonded monatomic sheets along the c-axis in the sequence –Te(1)–Bi–Te(2)–Bi–Te(1)–Te(1)–Bi–Te(2)–Bi–Te(1). Two different crystallography of Te atomic sites is present in Bi_2Te_3. Te atoms in Te(2) atomic sites form covalent bonding with the six nearest Bi atoms, while Te atoms in Te(1) atomic sites are bonded to three Bi atoms by covalent bonding and three Te atoms by Van der Waals bonding. Te(1)-Te(1) van der Waals forces connect the quintuple layers to form the Bi_2Te_3 structure. Because of this crystal structure, the lattice constant of the c-axis (3.045 nm) is approximately seven times as large as that of

the a, b-axis (0.439 nm) [51]. This is the reason for the anisotropic behaviour of Bi_2Te_3. The physical and chemical properties of Bi_2Te_3 is given in table 1.

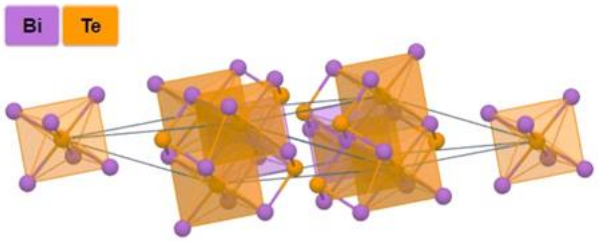

Figure 2. Crystal structure of Bi_2Te_3. (Image source: materialsproject.org/materials/mp-34202/)

Table 1. Summary of the physical and chemical properties of Bi_2Te_3 [52]

Compound Formula	***Bi_2Te_3***
Molecular Weight	*800.76*
Appearance	*Gray to black solid*
Melting Point	*585°C (1085°F)*
Density	*7.64 - 7.74 g/cm^3*
Solubility in water	*Insoluble*
Group	*Bismuth - 15, Tellurium - 16*
Lattice constant	*a = 0.4395 nm, c = 3.045 nm*
Unit cell	*Trigonal*
Crystal Structure	*Hexagonal - Rhombohedral*
Band Gap	*0.21 eV*

The performance of nanosized Bi_2Te_3 materials with excellent thermoelectric performance have been studied over the years. The high performance is mainly attributed to the effects of the low dimensionality and the reduction of the lattice thermal conductivity. The various low-dimensional structures of Bi_2Te_3 that have been studied so far are nanoparticles, nanoplates, nanocrystalline films, nanorods, nanotubes, nanowires and nanoflowers. A summary containing as this information has been presented in Table 3.

1.3.2. Antimony Telluride - Sb_2Te_3

Antimony Telluride, Sb_2Te_3, is a p-type semiconductor with a structure like Bi_2Te_3. The most important feature of Sb_2Te_3 that makes it suitable for low temperature applications is that the composition of Sb_2Te_3 can be manipulated to maximize the figure of merit. Sb_2Te_3 is an indirect narrow-gap semiconductor that has a rhombohedral crystal structure with symmetry space group R-3m. Sb_2Te_3 consists of a layered structure and each layer consists of five atomic planes ordered in the following sequence: Te1 -Sb-Te2 -Sb-Te1 , where Te1 and Te2 denote the positions of Te atoms as in Figure 3.

These layers is held together by weak Van-der-Waals interaction, which provide the interesting physical properties in Sb_2Te_3. Sb_2Te_3 shows a p-type conductivity which makes is very compatible with the n-type Bi_2Te_3 for making a device [53]. The physical and chemical properties of Sb_2Te_3 is given in table 2.

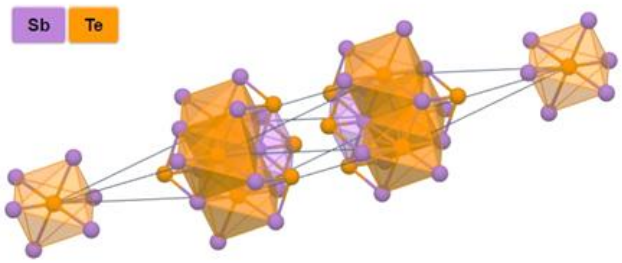

Figure 3. Crystal structure of Sb_2Te_3. (Image source: materialsproject.org/materials/mp-1201/)

Table 2. Summary of the physical and chemical properties of Sb_2Te_3 [54]

Compound Formula	***Sb_2Te_3***
Molecular Weight	*626.32 g/mol*
Appearance	*Gray solid*
Melting Point	*620°C (1148°F)*
Density	*6.50 g/cm^3*
Solubility in water	*Insoluble*
Group	*Antimony - 15, Tellurium - 16*
Lattice constant	*a = 0.4262 nm, c = 3.0435 nm*
Unit cell	*Trigonal*
Crystal Structure	*Hexagonal - Rhombohedral*
Band Gap	*0.28 eV*

The interest in exploring Sb_2Te_3 as an exceptional p-type thermoelectric material has been studied over the years. The various low-dimensional structures of Sb_2Te_3 that have been studied so far are nanoparticles, nanoplates, nanocrystalline films, nanorods, nanotubes, nanowires and nanoflowers. The information about this has been summarized in Table 3.

Table 3. Survey of the synthesis methods, morphology and dimensions of particles, and reaction conditions of Bi_2Te_3 and Sb_2Te_3

Composition	Structure	Synthesis Method	Temperature and Time	Dimensions	Reference
Bi_2Te_3	Nanotubes	Ultrasonic-assisted hydrothermal	180°C for 48 h	Length: 500–1000 nm Diameter: 50–100 nm	48
Ag, Sb, Sn Doped Bi_2Te_3	Nanoparticles	Ultrasonic-assisted hydrothermal	200°C for 3 h	28-40 nm	89
Bi_2Te_3	Nanoparticles	Ultrasonic-assisted solvothermal	70°C for 16 h, 20 h and 40 h	10-20 nm	90
Bi_2Te_3	Thin film	MOCVD	450°C	-	59
Bi_2Te_3/Sb_2Te_3	2D superlattice and thin films	MOCVD	350°C	-	60
Bi_2Te_3	Nanowires and nanoribbons	VLS	275 - 290°C	NW diameters: 50 nm and 90 nm NW length: 4μm, NR length: 13μm, NR Width 200 nm, NR thickness 80 nm	62
Bi_2Te_3	Nanoparticles	Reverse micelle	-	10 nm	50
Bi_2Te_3	Nanoparticles and nanorods	Refluxing	100°C for 2-24 h	Np: 15-23 nm, NR length 100 nm Diameter: 20 nm	64
Bi_2Te_3	Nanowires	Electrodeposition	RT	Diameter: 250 and 40 nm	67
Bi_2Te_3	Nanoparticles	Co-precipitation	RT	60-90 nm	69
Bi_2Te_3	Nanoparticles	Chemical alloying	375°C- 400°C	80 nm	70
Bi_2Te_3	Nanosheets, nanorags, nano sheet-rod and nanorods	Solvothermal	100–180°C for 10–50 h	Nanosheets: 100 and 400 nm 200–400 nm Nanorag Thickness: 10 nm Sheet-Rod Length: 1μm Diameter: 200-400nm NR Diameter: 10–60 nm	71
Bi_2Te_3	Nanoparticles and nanowire	Solvothermal	150°C for 24 h	Np Diameter 15–20 nm, NW diameter: <100 nm NW length: 10 μm	72
Bi_2Te_3	Nanoparticles and nanorod	Solvothermal	100–180°C for 10–50 h	Np: 20–40 nm NR Length: 150 nm NR Width: 10 nm	73

Bi_2Te_3	Nanoparticles and nanoplates	Solvothermal	60°C, 120°C and 180°C for 16 h	Np: 30 nm	74
Bi_2Te_3	Nanoplates	Solvothermal	210°C for 24 h	Diagonal: 70–200 nm Thickness: 30 nm	75
Bi_2Te_3	Nanoflower	Solvothermal	180°C for 8 h	Width: 300-2000 nm Thickness: 30 nm	76
Bi_2Te_3	Nanoparticles	Hydrothermal	100°C for 48 h	10 nm	80
Bi_2Te_3	Nanotubes	Hydrothermal	150°C for 24 h	Diameter: 30–100 nm Length: μm	81
Bi_2Te_3	Nanosheets and nanoplates	Hydrothermal	120°C for 12 h	Diameter: 50 nm and 500 nm Thickness: 50 nm and 60 nm	82
Bi_2Te_3	Nanoplates	Hydrothermal	210°C for 24 h	Diagonal: 0.2–1 μm Thickness: 100 nm	84
Bi_2Te_3	Nanowire	Hydrothermal	65°C for 48 h	Diameter: 15–20 nm Length: 1 μm	83
Bi_2Te_3	Nanoplates, nanorods, and nanotubes	Hydrothermal	150°C, 180°C and 210°C for 24 h	NP Length: 200-800 nm NR Length: 2 μm Diameter: 20-80 nm NT Length: 1 μm Diameter: 10 nm	51
Bi_2Te_3	Nanorods and nanoflakes	Microwave-assisted polyol method	0.5–6 h	NR Width:20–50 nm NR length: 200–400 nm NF length: 90 to 150 nm	91
$Bi_{0.5}Sb_{1.5}Te_3$	Nanoplates	Hydrothermal	150°C for 24 h	Length: 100nm - μm Thickness: 30 nm to 100 nm	93
Bi_2Te_3/ Sb_2Te_3	Nanoplates	Refluxing	90°C for 18 h	Diameter: 13 - 80 nm	65
Sb_2Te_3	Nanoplates	Refluxing	120−180°C for 24 h	Length:700nm−3 μm. Thickness: 50-350 nm.	66
Sb_2Te_3	Nanoparticles	Refluxing	120°C for 6 - 12 h	<100 nm	53
Sb_2Te_3	Nanowires	Electrodeposition	RT	NW Length: 7 mm Diameter: 100 nm	68
Sb_2Te_3	Thin films	MOCVD	< 250°C	-	61
Sb_2Te_3	Nanowires	VLS	< 250°C	-	62
Sb_2Te_3	Nanowires	VLS	low to - 430°C	Length: 20 μm Diameter: 73 nm	63

Sb_2Te_3	Nanoplates	Solvothermal	30°C for 24 h	Length: 3–5 μm Thicknesses: ~100 nm	77
Sb_2Te_3	Nanosheets	Solvothermal	200°C for 12 h	Length: 200–300 nm Thickness:18–20 nm	78
Sb_2Te_3	Nanoplates	Solvothermal	200°C for 24 h	Length: 200-2000 nm Thickness: several tens of nm	79
Sb_2Te_3	Nanobelts	Hydrothermal	200°C for 24 h	Width: 1-3 μm Thickness: 100 nm	85
Sb_2Te_3	Nanobelts and nanosheets	Hydrothermal	180°C for 12, 16 and 24 h	-	86
Sb_2Te_3	Nanoplates	Hydrothermal	160°C for 48 h	Length: 300 nm Thickness: 35nm	87
Sb_2Te_3	Nanoplates	Hydrothermal	180°C and 230°C for 11 h	Length: 200-600 nm Thickness: 10-60 nm	88
Sb_2Te_3	Nanosheets	Microwave-assisted solvothermal method	200°C for 15 mins	Length: 300–500 nm Thickness: 50–70 nm	92

1.4. Thermoelectric Materials Synthesis

In order to obtain high figure of merit, the quality of the synthesized TE materials is of prime significance. Manufacture of high quality TE materials are largely dependent on the reaction method, reaction parameters – time, temperature, pH, and the choice of the precursors. In order to provide a sustainable manufacture solution for the TE materials the following parameters were given importance.

- energy efficiency
- waste generation
- safe solvents and chemicals
- scalable synthetic process

1.4.1. Reaction methods - Overview

There are two approaches for the fabrication and formation of nanostructure: top – down and bottom – up [7]. In top- down approach, the bulk structure is broken down to form the nanostructures. In the bottom-up approach, the nanostructure is formed by combining the atoms, molecules and/or nanoparticles from bottom up. For the synthesis of thermoelectric materials, top–down approach is not preferred as it is becoming outdated and control over the process is not possible. Ball milling has been a preferred method for the synthesis of thermoelectric materials [55]. One of the highest *zT* reported for thermoelectric materials via ball milling was 2.1 for Cu_2Se at 973 K and 1.14 for p-type $(Bi,Sb)_2Te_3$ at 323 K [56-57]. However, it has been observed that longer hours of ball milling can lead to agglomeration and damage the surface of the particles. Furthermore, the risk of contamination and the high cost of high energy for ball milling makes this method not suitable for this project [58]. The other chemical method for the synthesis of Bi_2Te_3 and Sb_2Te_3 TE materials are reverse micelle [50], MOCVD [59-61], VLS [61-63], refluxing [53, 64-66], electrodeposition [67-68], chemical reduction [69-70], solvothermal [71-79], hydrothermal [51, 80-88, 93], ultrasonic-assisted method [48, 89-90], microwave-assisted method [91-92] and many more. These chemical methods have the advantages of low cost, less device-dependence and large-scale synthesis, but control of the product morphology is a problem [83]. Of all the chemical methods mentioned, the solvothermal/hydrothermal methods have been mainly used to prepare the nanostructure form with different morphologies as given in Table 3. However, the reaction time in solvothermal/hydrothermal methods can range from several hours to days [72, 76, 82-83, 86-87]. This drawback can be dealt with the introduction of microwave energy.

1.4.2. Microwave assisted heating

In the electromagnetic spectrum, microwaves have a frequency in the range 0.3-300 GHz (in between infrared and radio waves). It is widely used for heating, communication, navigation, food processing, sensing and resonance spectroscopy and several applications in chemistry since 1986 [94]. Microwave technology is emerging as an alternative energy source for the chemical synthesis with the aim to reduce the reaction time from hours or even days, like the case with most wet chemical synthesis routes, to few minutes [95-96]. Microwaves speed up the chemical reaction by increasing the overall kinetics of the reaction as it relies on localized superheating. It has been reported that since microwave heating leads to kinetically driven reactants in the reaction, it thereby reduces the formation of agglomerates ensuring a narrow-size distribution [97]. Additionally, it has also been reported that the products obtained after the reaction are of superior nature in terms of quality and yield [98-99]. Thus, uniform structural, textural, and novel properties have been obtained by microwave assisted synthesis [100].

Microwave assisted heating works on the phenomenon of microwave dielectric heating. When a dielectric material is exposed to microwaves, the interaction of the material with the microwaves

transforms the microwave energy into heat. Microwave-assisted heating is based on dipolar and ionic conduction mechanisms [94].

- ***Dipolar rotation***

  In this, a polar molecule (like water, ethanol, ethylene glycol, etc.) produces heat from the microwaves. The polar molecules align themselves by rotating in the direction of the electric field, and in turn lead to a phase difference between the rotating direction and the field. This leads to molecular friction and collisions that give rise of the dielectric heating [94].

- ***Ionic conduction***

  In this, the ionic charged particles oscillate under the effect of the electric field, leading to an electric current. This current faces resistance because of the collision of the charged species with the other molecules or atoms, causing the materials to heat up [94].

The fundamental difference between microwave heating and conventional heating process is that in microwave heating, heat is generated internally within the material by the interaction of microwaves with the material, instead of originating from external heating sources then transferring the heat to the materials. In microwave heating, a given temperature can be reached at a short induction time, thereby accelerating the reaction (superheating), instead of slowly warming from room temperature [94-95].

At the nanoscale, the material´s properties are highly dependent on the size and shape which can be controlled by realising the appropriate synthetic methodologies. The growth of the particles is largely dependent on the thermodynamics and kinetics of the reaction design. Since, conventional thermal techniques are based on the conduction of heat from the reaction vessel to the reaction solvent and then to the reactant molecules, the issue of the quality of the nanoparticles and the uniformity of the particle size is raised. Microwave heating can address the problems of inhomogeneous heating in conventional thermal techniques as it delivers rapid initial heating, increased reaction kinetics, enhanced reaction rates, uniform particle size and narrow particle size distribution. This is also a sustainable, environmentally friendly, and economically viable heating method for the bulk production of nanomaterials [95, 101-102].

Microwave assisted synthesis has developed as an efficient bottom-up method for chemical synthesis over the past decade. Microwave energy can be paired with any of the existing synthesis routes in order to obtain a rapid, economical, simple and efficient method [103]. Common methods that have used microwave heating are hydrothermal [98, 104-105], solvothermal [92, 99], combustion [95, 97, 100-102, 106], reflux [107] and polyol [96]. A variety of nanomaterials have been synthesized with the assistance of microwave, like 0D structures [92, 97-99, 100-101, 105-106], 1D structures [95-96, 102, 107] and 2D structures [104]. A summary about the microwave assisted synthesis has been presented in Table 4.

Using microwave energy has made the reaction more cost effective [101], reduced the processing time [98], energy efficient [107], good possibility of large volume production and has led to uniform nucleation of the particles with improved crystallinity, pure phase structures, high yield and enhanced properties of the materials [96, 99]. Dong G. H. *et al*. have rapidly synthesized Sb_2Te_3 single-crystalline nanosheets by a microwave-assisted method at 200°C for 15 min using using $SbCl_3$, Na_2TeO_3 and hydrazine hydrate in ethylene glycol. They have prepared bulk sample of Sb_2Te_3 nanosheets by spark plasma sintering (SPS) and have reported a high zT of 0.58 at 420 K [92].

Microwave assisted hydrothermal syntheses are regarded as so-called green processes because they are energy-efficient [94]. The aqueous solutions are processed at a lower temperature, using an effective heating process with no release of particulate matter or greenhouse gases. This lack of harmful

environmental impacts of microwave assisted hydrothermal synthesis makes it a good and viable method for the commercial production of various nanomaterials [95]. In microwave assisted hydrothermal/solvothermal method, the reaction medium is sealed in a pressurized vessel and heated above its boiling point. Due to the thermal effects, microwaves form super-heated areas (sometimes called hot spots) as a result of interference patterns in closed spaces. This is related to the rapid heating and faster rate of reaction [94, 96]. Considering the benefits of microwave energy, for the purpose of this thesis, a microwave-assisted hydrothermal method will be studied to synthesize thermoelectric nanostructures. Thus, in summary, the advantages of microwave assisted chemical reactions are given as follows:

- Selective, volumetric, non-contact, high efficiency heating can be achieved
- Significant reduction in reaction time because of the rapid internal heating
- Energy efficient and environmentally safe
- Cost effective because of the shorter processing times
- Good quality, pure and homogeneous products with uniform particle size and improved properties
- Controlled reaction
- Silent and no exhaust gases are generated
- Large volumes can be produced in a single batch
- High yield of products indicating no wastage of initial precursors

Table 4. Survey of the several microwave (MW) assisted synthesis methods showing the shorter reaction time and variety of morphology of the particles

Composition	Structure	Synthesis Method	Time	Dimensions	Reference
Ag	Nanorods	MW assisted combustion	30 sec - 15 mins	5-25 nm	95
$ZnFe_2O_4$	Nanoparticles	MW assisted combustion	10 mins	41 nm	97
$CoFe_2O_4$	Nanoparticles	MW assisted combustion	15 mins	60 nm	100
ZnO	Nanoparticles	MW assisted combustion	10 mins	10 nm	101
CuS	Nanorods	MW assisted combustion	20 mins	Length: 30-60 nm Thickness: 5-10 nm	102
SnO_2	Nanoparticles	MW assisted combustion	10 mins	10-20 nm	106
Ag	Nanowires	MW assisted polyol	3.5 mins	45 nm - few μm	96
SnO	Nanoparticles	MW assisted hydrothermal	2-6 h	30 nm- 2 μm	98
$BiFe_xCr_{1-x}O_3$	Thin Film	MW assisted hydrothermal	4 mins	-	104
CuO	Nanoparticles	MW assisted hydrothermal	5-30 mins	500 nm - 1 μm	105
Ag	Nanoparticles	MW assisted solvothermal	3 h	10 nm	99
Sb_2Te_3	Nanosheets	MW assisted solvothermal	15 mins	Length: 300–500 nm Thickness: 50–70 nm	92
V_2O_5	Nanorods	MW assisted reflux	1 h	1 μm	107

1.4.3. Reaction Parameters

The usage of large amounts of conventional volatile solvents in a chemical reaction for the synthesis of nanomaterials have been a pressing issue environmentally as well as economically. In this thesis, a major focus has been given to the choice of the reaction solvent and precursors. It was aimed to minimize the use of toxic chemicals and look for alternative sources. For this reason, it was a conscious decision to use water as the reaction solvent, instead of the most common solvent - ethylene glycol. Water is the perfect green solvent and several researches focussing on water as a medium to perform chemical reactions has been explored [71, 83, 105, 108]. When water is heat under pressure at temperatures between the usual boiling point, 100°C, and the critical temperature, 374°C, it is known as superheated water, subcritical water or pressurized hot water. Under microwave heating, the superheating of water causes the hydrogen bonds to break easily and the self-ionization of water increases with temperature. Superheating changes the properties of water making it less polar and it behaves more like an organic solvent such as polyol, methanol, ethanol, toluene, etc. [91] Zeynizadeh B. *et al*. have demonstrated the role of water as a green and good solvent for transferring electromagnetic energy into heat and thus driving the reduction reaction effectively [108]. The dielectric constant of the solvent has an important influence on the growth of the particles. In a solvent with low dielectric constant, the growth of the small bismuth telluride particles is steadier than in a solvent with a high dielectric constant [71]. The dielectric values of water with increasing values of temperature 100°C, 120°C, 150°C, 180°C, 200°C, 220°C, 250°C, 280°C and 300°C are 55.39, 50.5, 43.89, 38.10, 34.59, 31.32, 26.29, 22.45 and 19.66 respectively. The dielectric constant of water decreases at high temperatures (above its boiling point) [109]. Thus, these changing properties of water at elevated temperatures make it a good solvent for the synthesis of TE materials.

$BiCl_3$, $SbCl_3$ and Na_2TeO_3 have been chosen as the primary sources for Bi, Sb and Te ions respectively because they can be fully dissolved in water [48, 72, 76-78, 81, 84]. $BiCl_3$ and $SbCl_3$ are used because they can be effectively reduced to their respective ions with heating arrangement. For the Te ion, pure Te and Na_2TeO_3 are the common sources. Na_2TeO_3 has been chosen for this experiment because it has better solubility in water than Te [76, 83]. EDTA has been used as the structure directing agent in order to obtain the Bi_2Te_3 and Sb_2Te_3 nanostructures. Wang Z. *et al.* had used different surfactants like EDTA, polyvinyl pyrrolidone (PVP), sodium dodecyl-sulfate (SDS), and cetyltrimethyl ammonium bromide (CTAB) to synthesis of Bi_2Te_3 nanotubes. They have reported that longer reaction duration was needed when PVP and SDS were used as surfactant and no impurity because of EDTA was observed in the diffraction peaks [48]. Also, EDTA is one of the least hazardous chemical when compared to CTAB and SDS. Deng Y. *et al.* have synthesized various morphologies of Bi_2Te_3 nanocrystals by solvothermal process at 100-180°C for 10-50 h and reported that using EDTA leads to the formation of nanosheets and SDS/CTAB leads to the formation of nanorags [71]. It has been reported that EDTA serves as a bridging agent to form the multinuclear bismuth complexes and EDTA molecules can self-assemble to lamellar phases leading to the formation of Bi_2Te_3 sheet nuclei, which facilitates the formation of the nanoflakes and nanotubes [48, 84]. The role of EDTA in the formation of Bi_2Te_3 and Sb_2Te_3 have been investigated by various groups [64, 81, 87, 90]. Also, the activity of EDTA is dependent on the pH of the solution [80-88]. Thus, by changing the pH, the EDTA can lead to the formation of different morphologies of Bi_2Te_3 and Sb_2Te_3.

It has been reported that an alkaline medium is required for the formation of Bi_2Te_3 and Sb_2Te_3 nanostructures and a pH less than 11-12 should be maintained [73, 80, 82-84, 89, 91]. The alkaline medium makes the tellurium disperse in the reaction medium as telluride (Te^{2-}), which is beneficial for the formation of nanocrystals [76]. The formation of the Bi, Sb and Te ions requires the presence of a good reducing agent. Ethylene glycol (EG), hydrazine and are commonly used reducing agent but they are slightly harmful [82]. $NaBH_4$ is a mild reducing agent that has been known to reduce various

carbonyl compounds in water under microwave irradiation [108]. $NaBH_4$ as a reductant for the synthesis of Bi_2Te_3 and Sb_2Te_3 nanostructures has been reported by a lot of thermoelectric research groups [48, 51, 72, 75, 81-84, 87-89, 90]. $NaBH_4$ reacts with water with the evolution of hydrogen gas and reduces the precursors to their respective ions. At high pH, the activity of the reducing agent gets exhausted. NaOH is used as a pH regulator in the formation of the nanostructures. The importance of maintaining the pH for the formation of the thermoelectric materials has been studied and the role of NaOH has been appreciated in defining the morphology of the structures [51, 64, 76-77, 80-84, 88-90]. Im H. J. *et al.* have synthesized Sb_2Te_3 hexagonal nanoplates by solvothermal process at 230°C for 24 h and reported that when a small concentration of NaOH was used the particles formed were round, and as the concentration increased plate-like structures appeared [77]. Thus, higher the concentration of NaOH, the larger the particles produced, indicating the importance of an ambient value of pH for the reaction mechanism [64, 77]. It has also been reported that high concentrations of NaOH promote the anisotropic growth of Bi_2Te_3 [76]. Thus, in order to maintain the pH of the reaction medium, NaOH is used as the regulator.

Deng Y. *et al.* studied different morphologies of Bi_2Te_3 synthesized at 100-180°C by solvothermal process. They have reported that at low temperature and short reaction time, nanorods were observed and increasing the reaction temperature and time lead to the formation of spherical nanoparticles. They concluded that the particles, in general, became bigger with increasing reaction temperature and time [73]. Zhou *et al.* have prepared nanorods and nanoplates by microwave-assisted polyol method and they have reported that decreasing the reaction temperature slowed down the reaction, leading to smaller and more uniform particles of Bi_2Te_3 [91]. Stavila V. *et al.* have synthesized Bi_2Te_3 by solvothermal method and found that as the temperature increased from 60°C-120°C, the morphology changed from spherical nanoparticles to elongated plates [75]. Jin R. *et al.* have synthesized hierarchical flower-like Bi_2Te_3 through a facile solvothermal method. It was observed that as the temperature increased from 120°C-180°C, the aggregated nanoparticles decreases individually and a well-defined flower-like Bi_2Te_3 crystals formed [74]. Gupta S. *et al.* have reported that as reaction time increased from 2 h to 4 h, the particle size decreased from 26 nm to 18 nm [64].

As a general trend in Table 3 observing the reaction temperature of the hydrothermal/solvothermal methods for the synthesis of the different morphologies of Bi_2Te_3 and Sb_2Te_3, it can be deduced that low temperature is suitable for the reaction of nanoparticles, nanoplates and nanotubes and as the reaction temperature increases, the dimensionality changes from 0D to 1D. From Table 3, it can also be inferred that a reaction temperature ranging from 150-250°C is ideal for the synthesis of nanosheets, nanoplates, nanoribbons and nanofilms. By prolonging the reaction time, the different morphologies can be obtained. Thus, the effect of reaction time and reaction temperature are essential in determining the structure and morphology of the particles [79, 88]. The effect of reaction parameters on the morphology, structure, purity, and crystallinity of Bi_2Te_3 and Sb_2Te_3 nanocrystals in the light of thermoelectrics has been acknowledged and comprehensively studied in the academia and a summary is presented in Table 3.

An impressive work has been done by Stavila V. *et al.* to scale up the production of these nanoparticles with zT 0.38 at RT. They have found a new synthetic method to generate more than 10 g batches of near stoichiometric Bi_2Te_3 nanoparticles [75]. However, the use of a lot of hazardous and toxic chemicals like tri-noctylphosphine (TOP), 1-dodecanethiol, oleylamine and hydrazine hydrate makes this method environmentally harmful. In this thesis, we aim to achieve a method to scale up the production of the nanoparticles using less hazardous chemicals and a sustainable route of synthesis.

1.5. Research Methodology

In this section an overview about the different methods and methodologies that has been used in the thesis have been presented. A quantitative research method has been undertaken in this thesis that will help in the choice of research methods, strategies, data collection and analysis and an experimental approach has been applied. The microwave assisted synthesis method and the various characterization tools used in this thesis are analytical, fundamental and conceptual research methods wherein using the existing knowledge and findings from the literature survey has been studied. A theory about using water as a solvent for the nanoparticles growth instead of organic solvents has been formulated and the experiment has been designed to experimentally asses this. The alkalinity of the reaction medium has been challenged and by quantitative research in the synthesis process, this theory has been investigated.

A deductive approach has been established in this thesis for reasoning and testing the theories. The experiment is designed keeping in mind the work done previously and appropriate methods are adopted to synthesize, characterize, and measure the samples. The result is based on the analysis of the collected data and explanations of causal relationships between variables such as figure of merit, electrical conductivity, efficiency have been presented. The research strategies and designs are based on the information collected from the literature survey and to find plausible causal factors that can be changed to suit the scope of the thesis. An experimental approach has been used for data collection and descriptive and inferential statistics methods are used for data analysis. Different techniques like XRD, SEM, DLS are tested to obtain results about the structure and morphology of the samples.

In this thesis, the experimental methodologies are looked upon for the generation of the results. In order to establish the validity, reliability, and replicability of the thesis, a detailed flow of the experiment, a well-described procedure and consistency in obtaining the results from the measurements are presented. The dependability and transferability of the results are kept in mind so that the results can become a database for other researchers. With the aim of providing a green nanotechnology solution for large scale production of Bi_2Te_3 and Sb_2Te_3, the research methodology has been to seek a green and simplistic method to produce nanocrystals of high crystal structure.

1.6. Objective

The objective of this thesis is to provide a facile, state of the art, sustainable solution for large scale production of Bi_2Te_3 and Sb_2Te_3 nanomaterials. These materials have been proven to show excellent TE properties at room temperatures and can be used for recovery of waste heat and generation of electricity. The aim is to design the reaction conditions along the lines of green chemistry and optimize the experiment by modifying the precursors and solvents, reaction conditions and synthesis route. Taking advantage of the unique microwave dielectric heating phenomenon, rapid heating and short reaction time, the aim is to form hexagonal nanoplates of Bi_2Te_3 and Sb_2Te_3. These low dimensional structures have been efficient in enhancing the charge transport properties and electrical conductivity. A green, high yielding and low hazardous synthesis route has been followed to produce efficient and cost-effective TE nanomaterials with high crystallinity and pure phase crystal structure. Water is used as the solvent for the reaction instead for organic solvents making the reaction green, safe and non-hazardous. Another objective is to determine the value of pH required for the formation of the nanostructures without any impurities and high yield of the products. The structural properties, morphology and surface chemistry of these structures have to be studied to get information about the quality of the TE materials.

Chapter 2

Experimental Section

2.1. Material Synthesis

In this thesis, Bi_2Te_3 and Sb_2Te_3 TE nanostructures have been synthesized by a novel bottom up chemical method. In the synthesis, the focus has been to produce Bi_2Te_3 and Sb_2Te_3 nanostructures using green chemistry and green nanotechnology. The 12 Principles of Green Chemistry have been taken into consideration while designing the experiment [13]. Multiple batches of Bi_2Te_3 and Sb_2Te_3 had been synthesized to determine the optimal reaction conditions for the production of high quality Bi_2Te_3 and Sb_2Te_3 TE nanostructures. Microwave assisted synthesis has provided a simple, green and rapid process for the generation of these nanostructures.

A Milestone flexiWAVE microwave system has been used for heating. It allows high pressure synthesis as well as solid-phase reactions and has an inbuilt magnetic stirrer. It is useful to design and optimize synthetic processes as well as scaling up to multi-gram production. The flexiWAVE's microwave cavity has a volume of 70 litres and is equipped with two 950-Watt magnetrons for a total of 1900 Watt. The temperature can be monitored by fiber optic and infrared sensors. A contact-less sensor can be used to control each and every vessel, and the actual temperature values are shown on the instrument control terminal to allow an instant visual check of the reaction conditions. A picture of the microwave used in this project is given in Figure 4.

Figure 4. Milestone flexiWAVE Advanced Flexible Microwave Synthesis Platform

For obtaining a good morphology, apart from a structure directing agent, the precise reaction time and temperature are required. Because microwave is used for the synthesise, rapid heating is expected. A temperature of 220°C has been found accurate since it compliments with the low temperature reactions and microwave energy. After experiences from earlier work and few trials, a ramp time of 4 minutes and dwell time of 2 minutes has been decided. The 4 minutes ramping time is the minimum time required for the homogeneous distribution of heat in 1-4 reaction vessels when heated simultaneously in the microwave. Since we do not require large particles, the dwell time is kept short and tuned from reactions done previously in this microwave system that have provided substantial results.

All the precursors were stoichiometrically weighted and calculated as precisely as possible for the synthesis of the TE nanostructures. All the chemicals used for the synthesis were of analytical grade obtained from Sigma Aldrich and used as received without further purification: bismuth chloride, ($BiCl_3$ with ≥98% purity), antimony chloride, ($SbCl_3$ with ≥99.95% purity), sodium tellurite, (Na_2TeO_3 with 99% purity), sodium hydroxide (NaOH with ≥97.0% purity) and sodium borohydride ($NaBH_4$ with 98% purity). $BiCl_3$, $SbCl_3$ and Na_2TeO_3 were used as the precursors for Bi, Sb and Te ions, respectively. Deionized water was used as the solvent, EDTA as the structure directing agent, $NaBH_4$ as the reductant and NaOH to control the pH value of the solution.

As a general guideline, all the chemicals were handled based of the material safety data sheet and laboratory regulations. All the measurements of the chemicals while weighing and preparing of the solution was performed in the fume hood for safety. A one-step procedure of adding all the chemicals in one reaction vessel was followed instead of preparing multiple solutions and mixing them together in order to avoid any spillage or loss of material. Keeping in mind the empirical formula of Bi_2Te_3 (Sb_2Te_3), the molar ratio of 2:3 was used for the concentration of Bi and Te (Sb and Te) taken from their respective precursors. An alkaline medium was maintained during the reaction for the formation of Bi_2Te_3 and Sb_2Te_3.

The aim was to synthesise 1 g -2 g (small and big batch) of the final product in one reaction vessel and depending on the number of vessels used for a single run in the microwave the final yield of the batch was decided. One important thing that had to be kept in mind was that the energy inside the microwave chamber differed with the number of reaction vessels used and the concentration inside the reaction vessels. Initially, we have used 4-5 reaction vessels in the microwave each containing 1 g of the contents. The problem was all the reaction vessels were not receiving the same amount of heat and the heating profile of each of the reaction vessel were different. It was observed that few reaction vessels had a solution which was purple in colour, while some had a distinct separation between the water and particles. Thus, taking into consideration the distribution of heat inside the microwave, two reaction vessels were used inside the microwave containing the reagents. The difference in heat because of the number of reaction vessels and their contents played a huge role in optimising the reaction conditions.

2.1.1. Sample preparation of Bi_2Te_3 - small batch synthesis

a). Initially, for the preparation of 1 g of sample in each reaction vessel, we had prepared the sample solution by adding the precursors: 0.0384 M $BiCl_3$ and 0.0576 M Na_2TeO_3 in the reaction vessel along with the other chemicals – 0.6 g EDTA (0.03 M), 0.6 g $NaBH_4$ (0.2 M) and 0.6 g NaOH and this was followed by the addition of 80 ml DI water. The solution was alkaline in nature and the reaction vessel was kept under constant magnetic stirring for 30 minutes. This was then subjected to microwave heating at 220°C with ramp time of 4 minutes and dwell time of 2 minutes. This marks the end of the reaction inside the microwave. One sample was purple in colour after synthesis and is marked *SW_1a*. The sample in which clear water is obtained at the top and particles separated at the bottom is marked as *SW_1b*. A summary of the colour of the solution is given in Table 5. The schematic of the synthesis procedure mentioned in *Section 2.1.1 a* is given in Figure 5a and its corresponding heating profile in the microwave is given in Figure 5b.This procedure is fairly simple, however, using this process the absence of purple colour is not reproducible and it is also difficult to control the pH of the solution.

Table 5. Observation of the colour of the solution after microwave assisted synthesis of Bi_2Te_3 by the process given in Section 2.1.1 a.

Sample name	***Colour of the solution***
SW_1a	*Purple*
SW_1b	*Clear. Good phase separation*

b). In order to be able to control the pH of the solution, some changes were made in the procedure of the sample preparation. The Bi and Te precursors were added in the reaction vessel along with 0.6 g EDTA (0.03 M) and 0.6 g $NaBH_4$ (0.2 M). Then the addition of water was done dropwise. This was continued till the liberation of H_2 or until the bubbling of water was stable. The solution was kept under constant magnetic stirring. Then NaOH was added to the solution under the magnetic stirring. Two different amounts of NaOH was used to monitor the pH value of the solution. Sample *SW_2a* had 0.2 g NaOH and *SW_2b* had 0.6 g NaOH. Then the two samples are placed inside the microwave at 220°C with ramp time of 4 minutes and dwell time of 2 minutes. The sample is then allowed to cool to room temperature. Sample *SW_2a* was colourless after the reaction whereas *SW_2b* was purple in colour. A summary of the colour of the solution and its corresponding pH is given in Table 6. The schematic of the synthesis procedure mentioned in *Section 2.1.1 b* is given in Figure 6a and its corresponding heating profile in the microwave is given in Figure 6b.

Table 6. Observation of the colour of the solution and its corresponding pH value after microwave assisted synthesis of Bi_2Te_3 by process given in Section 2.1.1 b.

Sample name	***NaOH used***	***pH***	***Colour of the solution***
SW_2a	*0.2 g*	*10 - 10.5*	*Clear. Good phase separation*
SW_2b	*0.6 g*	*12.5 - 13*	*Purple*

2.1.2 Sample preparation of Sb_2Te_3 – small batch synthesis

For the preparation of 1g of Sb_2Te_3 sample in each reaction vessel, we had prepared the sample solution by adding the precursors: 0.0398 M $SbCl_3$ and 0.0598 M Na_2TeO_3 in the reaction vessel along with the other chemicals – 0.6 g EDTA (0.02 M), 0.6 g $NaBH_4$ (0.2 M) and 0.6 g NaOH and this was followed by the addition of 80 ml DI water. The solution was alkaline in nature and the reaction vessel was kept under constant magnetic stirring for 30 minutes. The sample is kept for microwave heating at 220°C with ramp time of 4 minutes and dwell time of 2 minutes and then allowed to cool to room temperature. The colourless sample is marked as *SW_3*. The schematic of the synthesis procedure mentioned in *Section 2.1.2* is given in Figure 7a and its corresponding heating profile is given in Figure 7b.

2.1.3 Sample preparation of Bi_2Te_3 – large batch synthesis

We also wanted to produce thermoelectric materials more than 1 g. With this aim, we had followed the process mentioned in *Section 2.1.1b*. However, scaling up was not easy. It was not enough to change the concentration of the reagents, the reaction conditions also that to be optimized accordingly. 0.062 M $BiCl_3$, 0.093 M Na_2TeO_3, 1.2 g EDTA (0.05 M) and 1.2 g $NaBH_4$ (0.2 M) were all added in the reaction vessel. The addition of 80ml of DI water was done dropwise until the liberation of H_2 or until the bubbling of water was stable. Then NaOH was added to the solution under the magnetic stirring. Two different amounts of NaOH was used to monitor the pH value of the solution. Sample *SW_4a* had 0.3 g NaOH and *SW_4b* had 0.8 g NaOH. Then the two samples are placed inside the microwave at 220°C with ramp time of 4 minutes and dwell time of 2 minutes. The sample is then allowed to cool to room temperature. A summary of the colour of the solution and its corresponding pH is given in Table 7. The schematic of the synthesis procedure mentioned in *Section 2.1.3* is given in Figure 8a and its corresponding heating profile in the microwave is given in Figure 8b.

Table 7. Observation of the colour of the solution and its corresponding pH value after microwave assisted synthesis of Bi_2Te_3 by process given in Section 2.1.3.

Sample name	***NaOH used***	***pH***	***Colour of the solution***
SW_4a	*0.3 g*	*10 - 10.5*	*Clear. Good phase separation*
SW_4b	*0.8 g*	*>12*	*Purple*

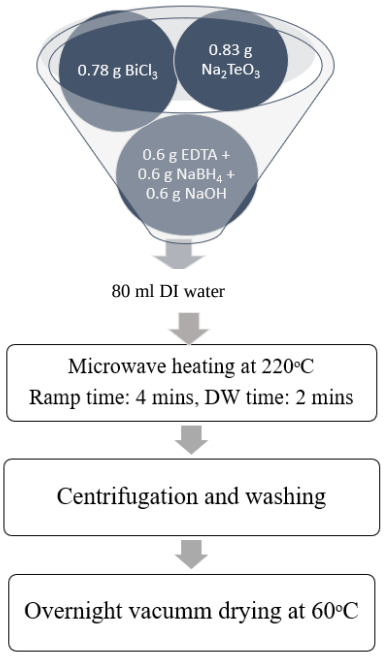

(a)

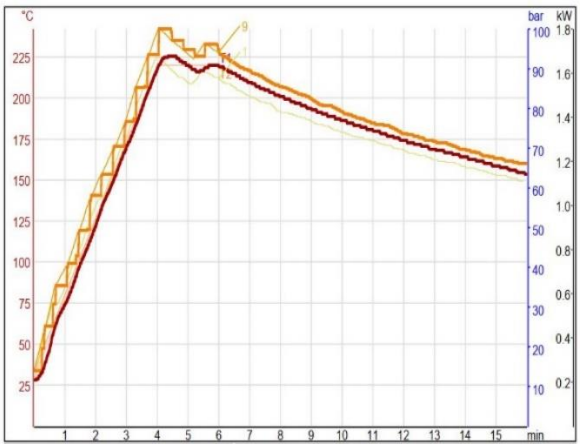

(b)

Figure 5 (a) Schematic of the microwave assisted aqueous chemical method with no control over pH used for synthesizing small batch of Bi_2Te_3 nanostructures by the procedure in Section 2.1.1 a. (b) The corresponding heating profile inside the microwave for the process given in Section 2.1.1 a

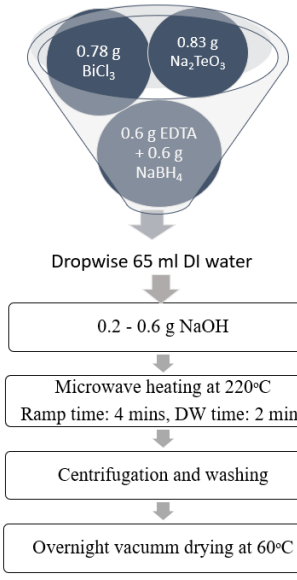

(a)

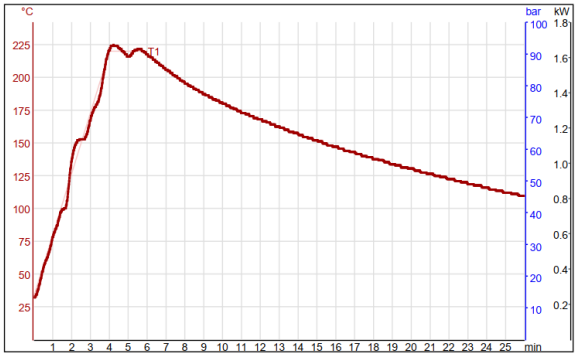

(b)

Figure 6 (a) Schematic of the microwave assisted aqueous chemical method with pH control for synthesizing small batch of Bi_2Te_3 nanostructures by procedure in Section 2.1.1 b. (b) The corresponding heating profile inside the microwave for the process given in Section 2.1.1 b.

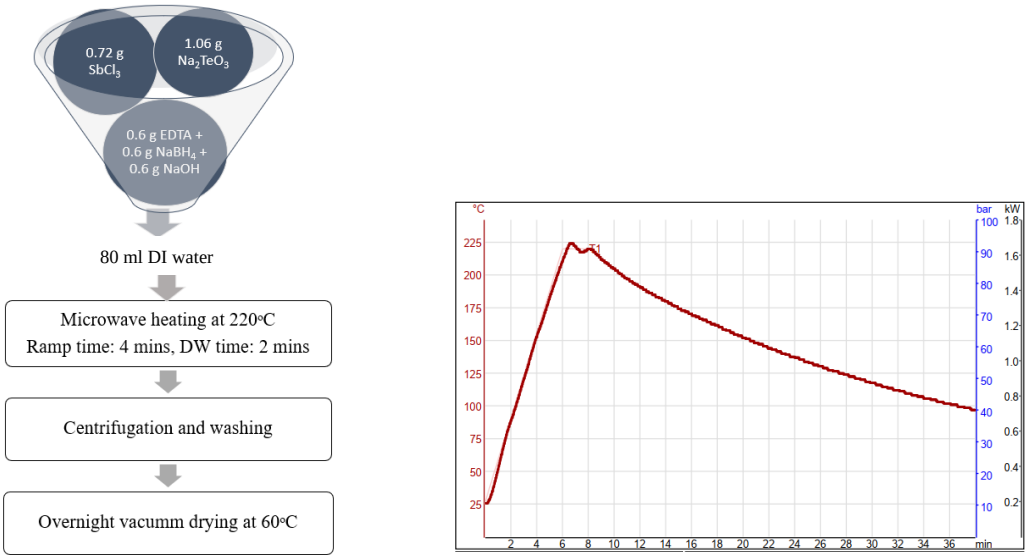

Figure 7 (a) Schematic of the microwave assisted aqueous chemical method for synthesizing small batch of Sb_2Te_3 nanostructures by procedure in Section 2.1.2. (b) The corresponding heating profile inside the microwave for the process given in Section 2.1.2.

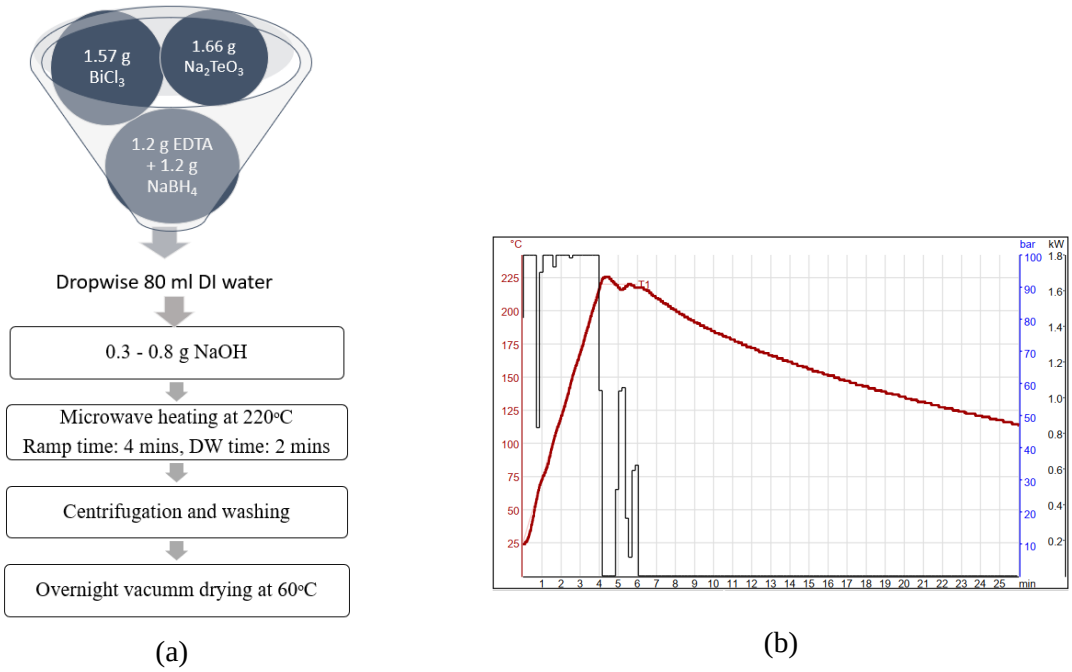

Figure 8 (a) Schematic of the microwave assisted aqueous chemical method with pH control for synthesizing large batch of Bi_2Te_3 nanostructures by procedure in Section 2.1.3. (b) The corresponding heating profile inside the microwave for the process given in Section 2.1.3.

(a) (b)

Figure 9 (a) Purple colour of the solution after synthesis indicating tellurium complexes as impurities. (b) Good phase separation observed with the particles precipitated at the bottom separated from the water.

While designing the experiment, the reaction parameters were optimized to obtain pure phase and high yield of the products while keeping in mind that the chemicals used in the process were safe, easy to handle and less hazardous. This water is chosen as the solvent for the reaction medium instead of EG, mild reducing agent $NaBH_4$ is used instead of hydrazine. Since a sustainable solution is being aimed at, the waste generated also must be managed. After the sample preparation, the washing procedure plays a critical role for the synthesis of the thermoelectric structures [70]. Thereafter, after the synthesis while the washing the precipitate, DI water, isopropanol and acetone are used during centrifugation instead of hexane, toluene, (more) thus reducing the organic pollutants in the environment. The clear water is obtained at the top of the solution can be easily removed, filtered, and repurposed or discarded as a safe inorganic solvent. The black precipitate is separated from the solution and washed thoroughly. Isopropanol, acetone and DI water were used for removing any unwanted functional groups from the final product. Usually, the black precipitate is washed thrice with DI water, once with isopropanol, once with acetone and lastly again with isopropanol. The reaction vessels are centrifuged for 5 min at a speed of 8000 RPM each time. After the washing process, the precipitate is vacuum dried at 60 °C overnight. Finally, the black powder is obtained and weighed.

2.2. Characterization Techniques

All the synthesized nanostructures have been characterized after the synthesis process to determine the nature and quality of the products. Several different techniques have been utilized to identify the crystallite phases, determination of composition, morphology studies and surface chemistry of the particles.

2.2.1. X-ray Diffraction (XRD)

The phase structures were investigated by X-ray diffraction (XRD) to identify the crystal structure, lattice parameters and crystallinity of the materials. Powder diffraction method was used for the analysis of the Bi_2Te_3 and Sb_2Te_3 nanostructures. XRD analysis was performed using a Philips PANalytical X'Pert Pro Powder Diffractometer with Cu *Kα* source (*λ=1.54 Å*). The interaction of the incident beams with the sample provides the diffracted beams that satisfies the Bragg's law:

$$n\lambda = 2dsin\theta \qquad \text{..... Equation 14}$$

where, λ is the wavelength of the x-rays to the diffraction angle (θ), the distance between the diffracted planes is given by *d* and *n* is the order of diffraction. The Miller indices *(hkl)* gives the planes in the crystal lattices, and using *(hkl)* and *d*, the lattice constants can be determined.

2.2.2. Scanning Electron Microscopy (SEM)

The particle morphology and structure of the samples were examined by SEM. It is a dynamic characterization tool used to obtain high-resolution microstructure images of materials. A focussed beam of electrons is used to interact with the atoms of the sample rising from elastic and inelastic scattering from the surface of the sample. High energy electrons, called backscattered electrons, ejected by the elastic collision of the incident electrons, are used for elemental composition. Secondary electrons are lower energy electrons emitted due to inelastic scattering by atoms near the surface of the sample and are useful for the inspection of the topography of the sample´s surface. The imaging of the samples was done by the FEI Nova 200 Dual Beam system equipped with a 30 kV SEM FEG column and a 30 kV FIB column with Gallium source. During the operation of the instrument, the working distance was maintained at 5mm and the accelerating voltage was 10 kV.

2.2.3. Dynamic Light Scattering (DLS)

DLS is a non-invasive technique for measuring the size and size distribution of particles in a suspension in the submicron region. In a suspension, the Brownian motion of particles causes laser light to get scattered at different intensities and analysing these intensity fluctuations yields the velocity of the Brownian motion. Brownian motion is inversely proportional to particle size, thus, the larger the particle, the slower is the diffusion. DLS measurement is a volume distribution and thus determining the particle size for a given volume of the solution is more effective that intensity distribution. The particle size and stability of the particles are proportional to the zeta potential. The zeta potential (also known as electrokinetic potential) is an interfacial property on the surface of any material when it comes in contact with a liquid medium. It signifies the effective net charge in this condition and is given in millivolt unit. Measurement of the zeta potential provides information on surface functionality, the stability of colloidal dispersion as well as interaction of dissolved compounds with the solid surface. The zeta potential is dependent on the pH of the solution or the ionic strength of the dispersant and measurement of zeta potential at different pH values gives information about the the sample's surface, *i.e*. the presence of acidic or basic functional groups. When the zeta potential for a value of pH becomes zero, it is known as the isoelectric point and it is an indicator of the surface chemistry of the suspended particles. Near the isoelectric point, the particles have low zeta potential which means the particles are least stable. The particles undergo destabilization, whereby, they coagulate, come together and form the aggregates. When the particles aggregate, as a function of the volume, the particle size decreases, and the surface area increases. As the zeta potential moves away from the isoelectric point, the particles become stable and the particle size increases as they are not agglomerated strongly. Zeta potential vs pH measurements were done using Malvern Zetasizer Nano ZS90 instrument.

Chapter 3

Results and Discussion

3.1 Particle morphology and crystal structure

Bismuth telluride (Bi_2Te_3) and antimony telluride (Sb_2Te_3) have been synthesized by a microwave assisted aqueous chemical solution method. After the reaction in the microwave, a preliminary observation can be made about the formation of the Bi_2Te_3 and Sb_2Te_3 nanostructures by the colour of the solution. The purple colour of the solution suggests the presence of polytellurides, NaTe and other tellurium complexes [84]. When the black particles settle at the bottom of the reaction vessel clearly separated from the water, it is certain that the correct phase of Bi_2Te_3 and Sb_2Te_3 nanostructures are formed as given in Figure 9.

Considering the synthesis method mentioned in *Section 2.1.1 a,* 1 g of Bi_2Te_3 is synthesized in 80 ml DI water at reaction temperature 220°C with ramp time of 4 minutes and dwell time of 2 minutes. *SW_1a* is purple in colour whereas *SW_1b* has a distinct separation between the particles and the water. The morphology and size of the as-synthesized products of *SW_1a* and *SW_1b* are characterized by a SEM. The SEM images of *SW_1a* and its XRD pattern are given in Figures 10 and 11, respectively. Also, the SEM images of *SW_2a* and its XRD pattern are given in Figures 12 and 13, respectively.

Figure 10 shows the SEM images of *SW_1a* and it a collection of hexagonal nanoplates of length varying from 400 nm to 1 μm and rod-like structure of hundreds of nanometres to tens of micrometres. The presence of rod-like structure is an indication that not all the tellurium has reduced to the telluride ions and thus the nanostructure of desired Bi_2Te_3 structure has not formed. The XRD pattern of *SW_1a* in Figure 11 shows that a rhombohedral lattice structure of Bi_2Te_3 is formed, however, it could be confirmed that the desired Bi_2Te_3 crystal structure has not formed as the significant peaks of Bi_2Te_3 are not present. From the analysis of the XRD pattern it has been found that the structure formed is Bi_4Te_3 (JCPDS #33-0216). It can also be observed that the XRD peaks are broadened and not as sharp. Broadening of XRD peaks is associated with the presence of impurities which can be confirmed from the rod like structures as seen in the SEM images from Figure 10 (a).

The SEM image of *SW_1b* given in Figure 12 reveals that the typical products consist of irregular structures mostly of hexagonal plate-like structures and nanoparticles. The hexagonal plates are 300 nm to 1 μm in diagonal and 20-70 nm in thickness and the nanoparticles are 40-100 nm in diameter. It can also be viewed from Figure 12 (c) that the hexagonal nanoplates have formed stacked structures along the c-axis which can be effective for the electron transport of these low dimensional structures. The XRD pattern in Figure 13 indicates that the microwave assisted aqueous chemical method synthesized powders have a rhombohedral lattice structure of Bi_2Te_3 space group of R-3m (JCPDS #15-0863). The lattice constants are $a = b = 4.38Å$ and $c = 30.49Å$, which are in agreement with the reported values. The main peaks originated from the *(006), (015), (10 10), and (00 15)* planes. The intensity gives an idea about the density of the particles and the crystallinity of the diffracted planes. The sharp peaks are also an indication about the purity in phase and the high crystalline nature of the Bi_2Te_3 nanostructure.

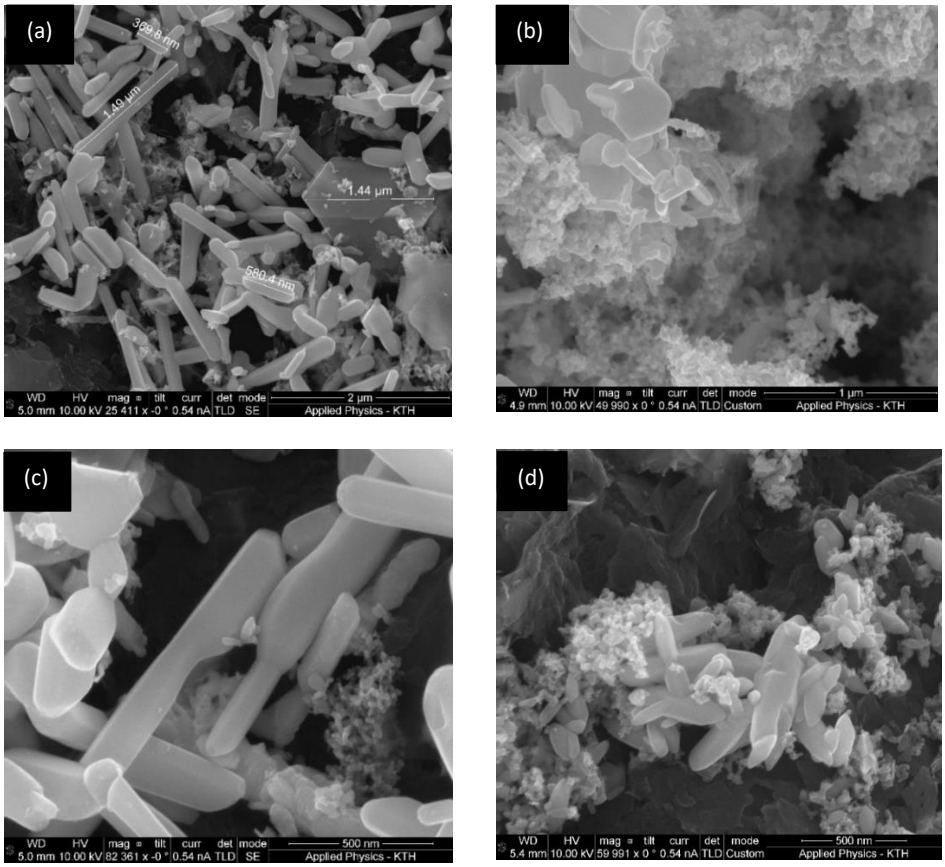

Figure 10. SEM images of different magnifications of SW_1a bismuth telluride nanostructures synthesized by a microwave assisted aqueous chemical method in 2 minutes dwell time at 220°C. Hexagonal nanoplates of length varying from 400 nm to 1 µm are observed with rod-like structures as impurities.

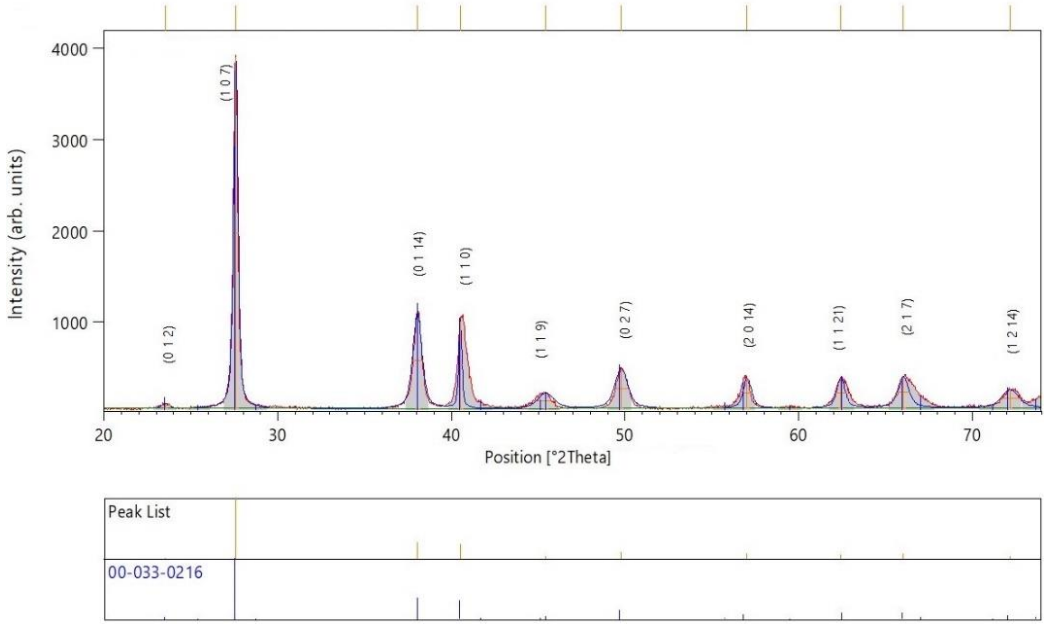

Figure 11. XRD of SW_1a bismuth telluride nanocrystal synthesized by a microwave assisted aqueous chemical method in 2 minutes dwell time at 220°C. JCPDS #33-0216 for reference for Bi_4Te_3.

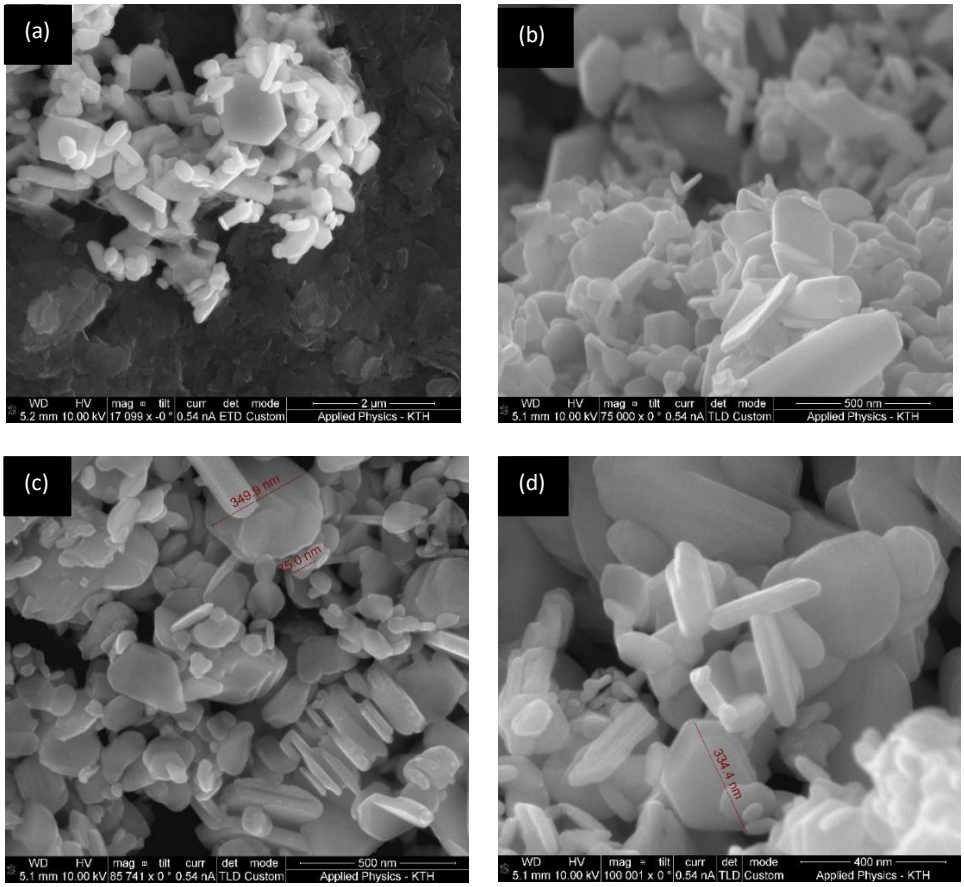

Figure 12. SEM images of different magnifications of SW_1b bismuth telluride (Bi_2Te_3) hexagonal nanoplates synthesized by a microwave assisted aqueous chemical method in 2 minutes dwell time at 220°C. The hexagonal plates are 300 nm to 1 μm in diagonal and 20 to 70 nm in thickness.

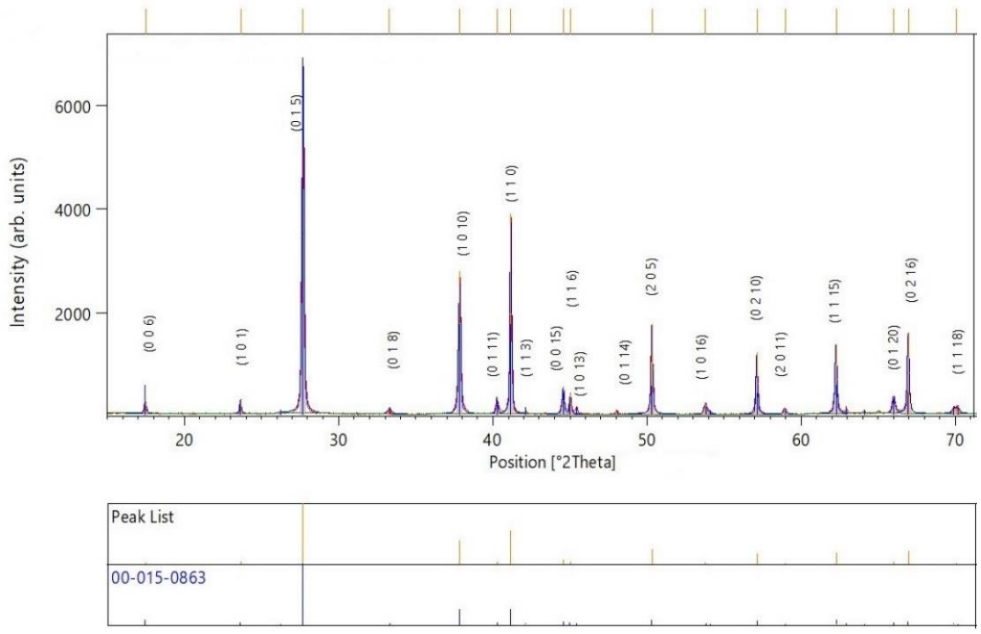

Figure 13. XRD of SW_1b bismuth telluride (Bi_2Te_3) nanocrystal synthesized by a microwave assisted aqueous chemical method in 2 minutes dwell time at 220°C. JCPDS #15-0863 for reference.

By the synthesis process in *Section 2.1.1 a*, multiple batches of samples have been prepared, however, the outcome has differed among samples in the same batch. This process does not account for reproducibility. Although the heating profile given for samples *SW_1a* and *SW_1b* are similar, one explanation is that the distribution of heat might not be uniform among all the reaction vessels in the microwave which could affect the kinetics of the reaction. This, however, does not provide a causal relationship between the two events. Also, the lack of control of the pH of the reaction solution does not help in obtaining reproducible results. In order to ensure the complete reduction of tellurium, it is important to gauge the role of the reducing agent. The reducing agent, $NaBH_4$, becomes stable at high pH and its activity gets exhausted before the completing the reduction of the metal ions. Thus, the pH of the reaction mixture must be monitored and NaOH is required as a pH regulator.

The samples *SW_2a and SW_2b* have been prepared by a modified process given in *Section 2.1.1 b* whereby the pH of the reaction mixture is monitored by controlling the amount of NaOH. The pH of *SW_2a* and *SW_2b* were 10-10.5 and 12.5-13, respectively. After the microwave heat treatment, the sample solution of *SW_2a* was clear with the water on top and the particles settled at the bottom and *SW_2b* was purple in colour. As discussed earlier, the purple colour is an indication of the incomplete reduction of tellurium and a highly alkaline medium is not suitable for the formation of Bi_2Te_3 nanoparticles. The formation of Bi_2Te_3 requires the reduction of the precursors in a certain alkalinity of the soluble substances. Thus, the optimisation of the pH is required for the formation of pure Bi_2Te_3 structures.

The SEM images and XRD pattern of sample *SW_2a* are given in Figures 14 and 15 respectively. The morphology of sample *SW_2a* Bi_2Te_3 nanostructures in Figure 14 is a mix of nanoparticles and hexagonal nanoplates. The hexagonal nanoplates have a length around 180-800 nm and thickness ranging from 20-50 nm, and the diameter of the nanoparticles in the size distribution 30-70 nm. The stacked structures formed by the hexagonal nanoplates as seen in Figure 14 (c-d) can be as a result of the heterogeneous nucleation of the nanoplates and might be an aid in the transport properties.

Comparing the Figures 12 and 14, it can be observed that both the thickness and side length of sample *SW_1b* are larger than those of sample *SW_2a*. This reduced particle size can be due to the comparative low pH of the sample *SW_2a*. This reduced size can significantly show improved thermoelectric performance due to the reduction in thermal conductivity in these particles because of quantum size confinement. It can also be observed that the hexagonal plates are more regular in Figure 14 than in Figure 12. This is because the reaction medium has a pH between 10 and 11 which is suitable for EDTA to form lamellar phases and due to the strong hydrogen interactions among the EDTA molecules, the complexes can self-assemble to sheets leading to the formation of Bi_2Te_3 sheet nuclei.

The XRD pattern of *SW_2a* given in Figure 15 demonstrates the main peaks of Bi_2Te_3 at *(006), (015), (10 10), and (00 15)* planes are present and all the peaks can be indexed to rhombohedral Bi_2Te_3 with space group R-3m (JCPDS # 15-0863). No other crystalline impurities are detected, indicating the phase purity of the Bi_2Te_3 product and the high intensity shows the high crystallinity of the diffracted planes of Bi_2Te_3. The diffraction peaks of sample *SW_2a* are much sharper than those of *SW_1b*, indicating better crystallinity of Bi_2Te_3 formed by controlling the pH of the reaction mixture. Thus, by monitoring the pH of the solution to around 10-10.5, a suitable reaction environment was designed to produce high quality Bi_2Te_3 nanoparticles.

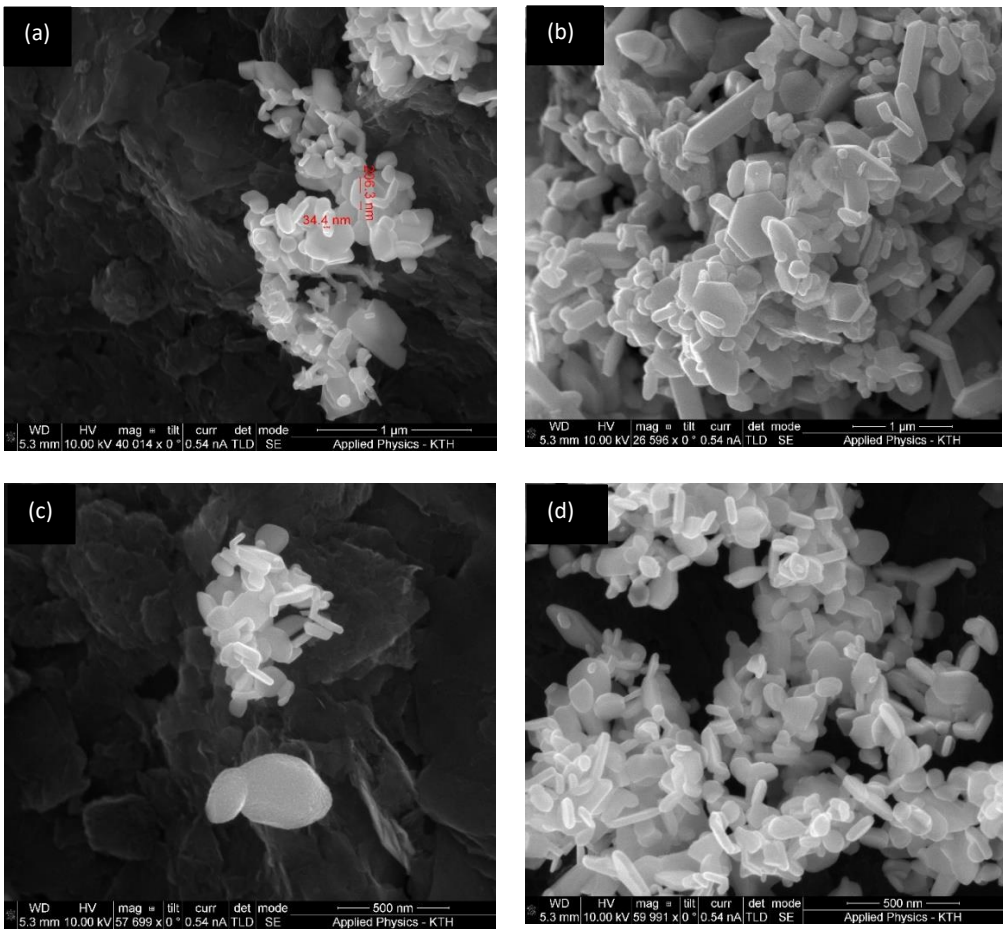

Figure 14. SEM images of different magnifications of SW_2a bismuth telluride (Bi_2Te_3) hexagonal nanoplates and nanoparticles synthesized by a microwave assisted aqueous chemical method in 2 minutes dwell time at 220°C. The hexagonal nanoplates are 180 to 800 nm in length and thickness ranging from 20 to 50 nm, and the diameter of the nanoparticles are 30-70 nm.

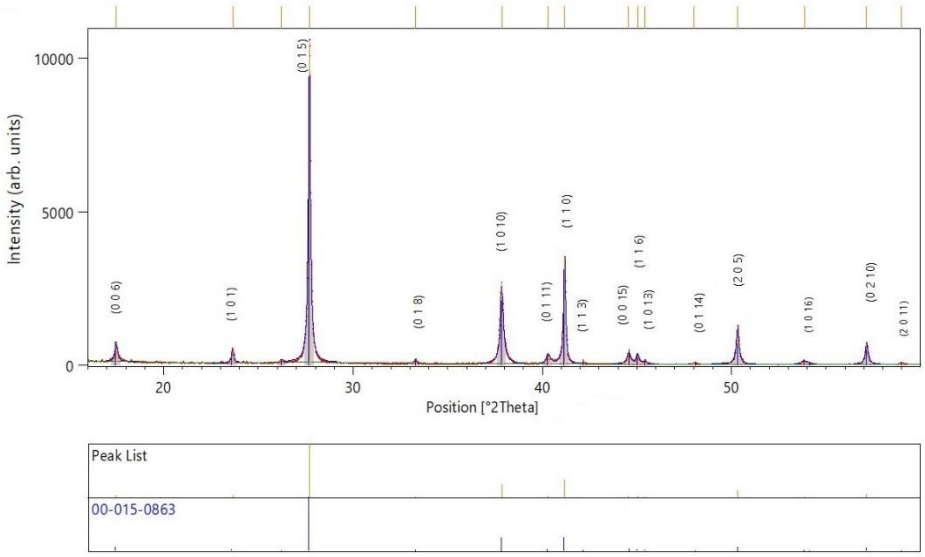

Figure 15. XRD of SW_2a bismuth telluride (Bi_2Te_3) nanocrystal synthesized by a microwave assisted aqueous chemical method in 2 minutes dwell time at 220°C. JCPDS #15-0863 for reference.

Sb_2Te_3 nanostructures have been synthesized by microwave heating for 2 minutes at 220°C in an aqueous environment using water as the solvent by the procedure mentioned in *Section 2.1.2*. The SEM images and XRD of sample *SW_3* are given in Figures 16 and 17, respectively. Figure 16 shows a wide distribution of closely bound regular hexagonal nanoplates. The morphology consists of smaller and larger plates having edge lengths as small as 80 nm to approximately 1 μm and thickness ranging from 30 to 120 nm. The presence of micro and nanostructures can provide an improved pathway for the conduction of the charge carriers along the grain boundary. The stacked arrangement is also formed in Sb_2Te_3 as seen in Figure 16 (b-c). The SEM image in Figure 16 (a) also show that the plates cut across one another which might be helpful for improved phonon scattering and electron transport. Figure 17 shows the XRD patterns of the as-prepared Sb_2Te_3 nanoplates and the diffraction peaks can be well indexed to the rhombohedral Sb_2Te_3 structure (JCPDS #01-071-0393). No peaks of Te or Sb_2O_3 was detected, indicating the formation of single phase Sb_2Te_3 without the presence of any impurity phase. The sharp XRD peaks gives an indication of the high crystallinity of the Sb_2Te_3 nanoplates.

An attempt has been made to scale up the production of Bi_2Te_3 by monitoring the pH and sample *SW_4* has been prepared by microwave heating. The SEM images are given in Figure 18 and the morphology is a mixture of regular and irregular hexagonal nanoplates, irregular nanoparticles and some large plate-like structures. The hexagonal nanoplates are 50-900 nm in diagonal with thickness ranging from 30-70 nm and the irregular nanoparticles are 40-70 nm in diameter. The large plate-like structures are 700 nm-1 μm wide and seem thinner than the hexagonal nanoplates. These large plates are impurities or unreacted products that have been formed. Figure 19 shows the XRD patterns of *SW_4* prepared by microwave assisted method. The detected peaks can be indexed to R-3m rhombohedral lattice structure (JCPDS #15-0863). However, one peak at 2Theta = 30.82° does not fit in the structure and is found to be a peak of Bi_2TeO_5 (JCPDS #24-0154). This corelates with the SEM images in Figure 18 (b) indicating that the large plate-like structures are Bi_2TeO_5 plates. The SEM and XRD have been conclusive to show that pure Bi_2Te_3 nanostructures have not been obtained and the reaction conditions need to be optimized further to obtain scalable high quality Bi_2Te_3 nanostructures.

A summary about the discussion of the colour of the solution samples, composition, morphology and nature of the Bi_2Te_3 and Sb_2Te_3 nanostructures has been given in Table 8.

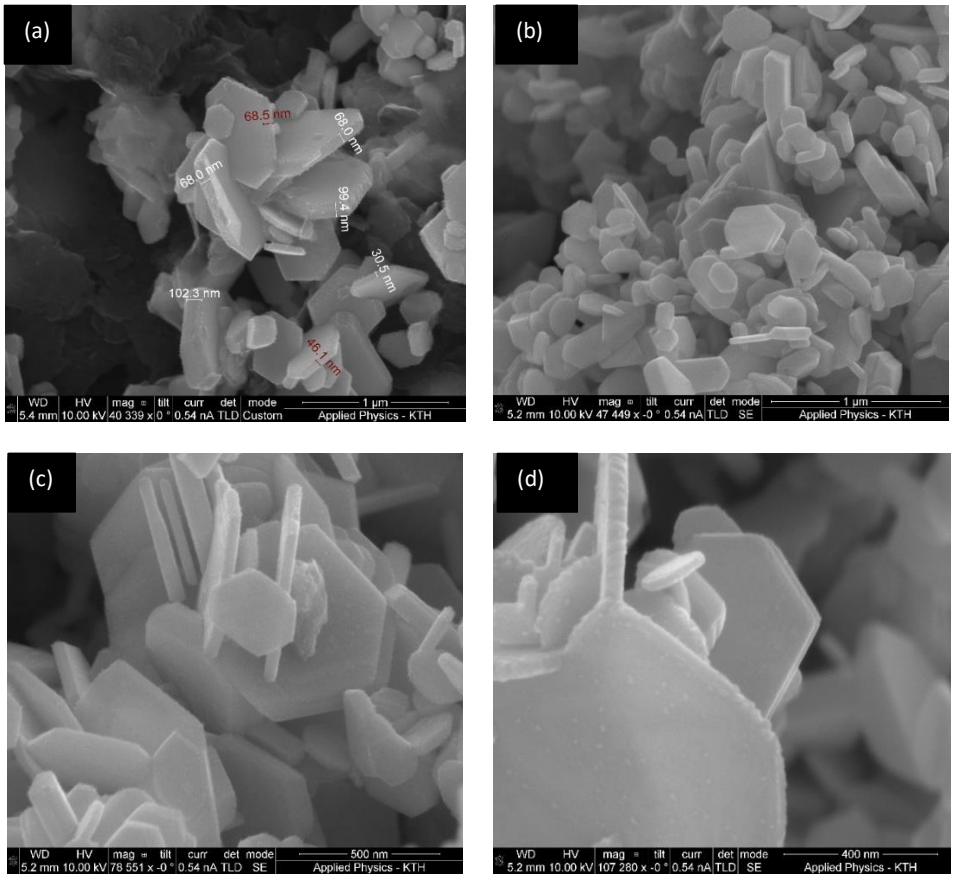

Figure 16. SEM images of different magnifications of SW_3 antimony telluride (Sb_2Te_3) hexagonal nanoplates synthesized by a microwave assisted aqueous chemical method in 2 minutes dwell time at 220°C. The hexagonal plates edge lengths are 80 nm to 1 μm and thickness ranging from 30 to 120 nm.

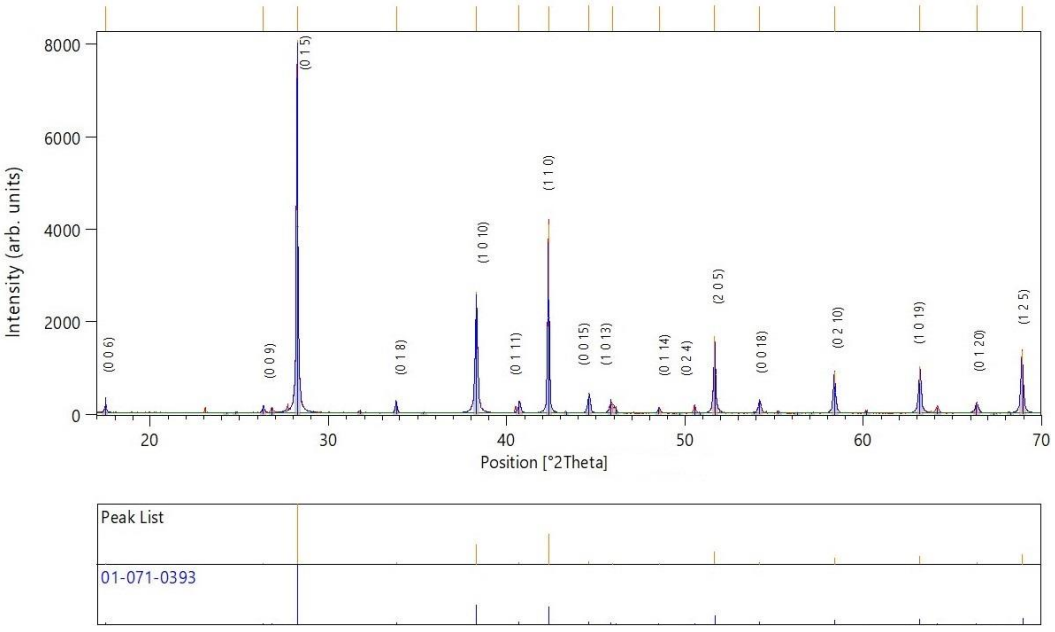

Figure 17. XRD of SW_3 antimony telluride (Sb_2Te_3) nanocrystal synthesized by a microwave assisted aqueous chemical method in 2 minutes dwell time at 220°C. JCPDS #01-071-0393 for reference.

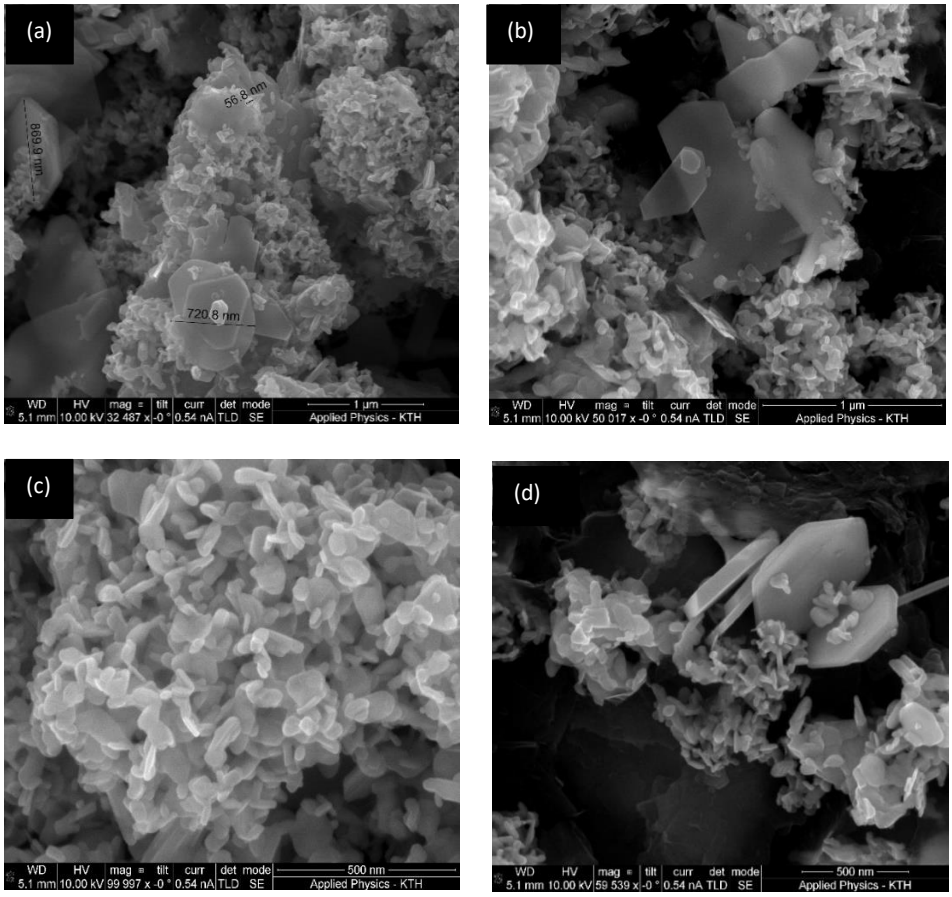

Figure 18. SEM images of different magnifications of SW_4 bismuth telluride (Bi_2Te_3) hexagonal nanoplates and nanoparticles synthesized by a microwave assisted aqueous chemical method in 2 minutes dwell time at 220°C. The hexagonal nanoplates are 50-900 nm in diagonal with thickness ranging from 30-70 nm.

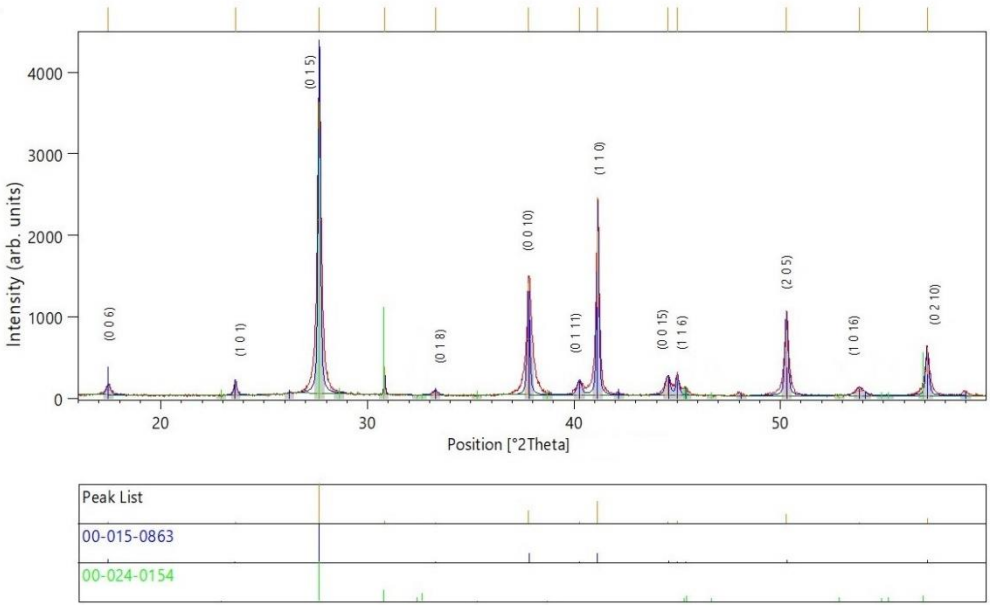

Figure 19. XRD of SW_4 bismuth telluride (Bi_2Te_3) nanocrystal synthesized by a microwave assisted aqueous chemical method in 2 minutes dwell time at 220°C. JCPDS #15-0863 for reference.

Table 8. A summary about the particle morphology, crystal structure and yield of the Bi_2Te_3 and Sb_2Te_3 TE nanostructures synthesized by microwave assisted heating at 220°C in 4 minutes ramp time and 2 minutes dwell time.

Sample Name	Colour of solution, pH	Composition	Structure	Dimensions	Yield
SW_1a	*Purple, pH -NA*	Bi_4Te_3	*Hexagonal nanoplates, Te rod-like structures*	*l = 400 nm- 1 μm t = 100 nm-1 μm*	*90%*
SW_1b	*Clear, pH -NA*	Bi_2Te_3	*Hexagonal nanoplates and nanoparticles*	*l =300 nm - 1 μm t =40-100 nm d =40-100 nm*	*92%*
SW_2a	*Clear, pH 10-10.5*	Bi_2Te_3	*Hexagonal nanoplates and nanoparticles*	*l =180-800 nm t = 20-50 nm d =30-70 nm*	*97%*
SW_3	*Clear, pH 14*	Sb_2Te_3	*Nanoplates*	*l =80 nm-1 μm t = 30-120 nm*	*89%*
SW_4	*Clear, pH 10-11*	Bi_2Te_3	*Hexagonal nanoplates, nanoparticles and large Bi_2TeO_5 plates*	*l =50-900 nm t = 30-70 nm d =40-70 nm w = 700 nm-1 μm*	*95%*

l = length of the nanoplate, t = thickness of the nanoplate, d = diameter of the nanoparticle, w= width of the large plates.

The visual observation of the purple colour of the solution is an indication about the purity of Bi_2Te_3 and Sb_2Te_3 TE nanostructures. The SEM images and XRD confirm the presence of impurities when the solution is purple instead of it being clear. The purple coloured solution is an indication of the incomplete reduction of tellurium to form the desired products. The presence of tellurium oxide, polytellurides and other tellurium complexes as impurities could reduce electrical conductivity causing degradation of thermoelectric efficiency in these TE materials [65]. The morphology and crystal structure of the microwave assisted synthesized hexagonal nanoplates are found to be almost equal to the ones from prepared hydrothermally, as observed from the literature survey (Table 3). This credits the rapid microwave heating which compresses the reaction time from long hours/days to few minutes.

The optimization of the value of pH required for the growth of the Bi_2Te_3 nanoplates is successfully done by modifying the experimental procedure. It has been found that an alkaline medium with pH under 11 is suitable for the growth of the hexagonal nanoplates as also reported by Novaconi, S. *et al.* [89]. The amount of NaOH required to monitor the pH was sufficient to maintain the ambient degree of alkalinity, which was required for the optimal function of - $NaBH_4$, the reducing agent and EDTA, structure directing agent. When these reaction parameters are subjected to the superheating by microwaves and ideal reaction temperature and time, pure phase, highly crystalline hexagonal Bi_2Te_3 and Sb_2Te_3 nanoplates and nanoparticles are formed.

3.2. Mechanism and growth of nanostructures

From observing the literature in Table 3 for the mechanism of the growth of the structures, it can be safely concluded that as the reaction time and temperature increases for low temperature reactions, the structure changes from nanoparticles to nanosheets/nanoplates to nanorods/nanotube [48, 79].

The Bi_2Te_3 and Sb_2Te_3 crystals grow predominantly along the *ab* plane direction because the strong covalent bonds between Bi-Te(2) and Sb-Te(2) can be easily extended along the plane. Along the *c-axis*, ionic and covalent bonds join the five hexagonal layers with Van der Waals force joining the quintuple layers perpendicular to c-axis. As the temperature in the microwave increases, the dielectric constant of water, the reaction solvent, reduces. This gives rise to dielectric heating. The low dielectric constant of the solvent provides steady growth of the small Bi_2Te_3 and Sb_2Te_3 crystals.

The possible mechanism for the formation of the TE Bi_2Te_3 and Sb_2Te_3 single crystal nanoplates by the microwave assisted method can be given in two processes: (Figure 20)

i. formation of tiny Bi_2Te_3/Sb_2Te_3 clusters as nascent crystal nuclei achieved during ramping
ii. subsequent crystal growth of plate-like structure from the nuclei under suitable conditions.

The hierarchical Bi_2Te_3/Sb_2Te_3 nanocrystals are fabricated through a self-assembly process. The selective adsorption of the precursor ions: $Bi^{3+}/Sb^{3+}$and Te^{2-} leads to the nucleation of the nanocrystals and tiny Bi_2Te_3/Sb_2Te_3 nuclei are formed. Te^{2-} ions first emerge with the reduction of TeO_3^{2-} followed by reaction with Bi^{3+}/Sb^{3+} ions, leading to the homogeneous/heterogeneous nucleation of Bi_2Te_3/Sb_2Te_3 nanoparticles and nanoplates. The nucleation occurs only when the concentration reaches the minimum saturation required to overcome the critical energy barrier (supersaturation) and nucleation rate increases rapidly as the concentration increases. Initially, rate of the electron transfer is linear with temperature. As the reaction process continues, the thermodynamic driving force increases but soon becomes limited by atomic mobility as temperature increases. The reactants Bi^{3+}/Sb^{3+} and Te^{2-} ions tend to dissolve away from the tiny particles and precipitate onto the surface of larger particles through dissolution- reprecipitation to become stable. This is due to Ostwald ripening. This causes a decrease in the total energy of the interface between the particles and the solution. The interface energy plays an important role in growth of pure phase rhombohedral R-3m unit cell with a hexagonal layer structure. Once nuclei are formed, growth occurs simultaneously and above the minimum concentration, nucleation and growth are inseparable processes, but they proceed at different speeds [84].

At this stage, in ambient alkaline medium, EDTA, the structure directing agent, starts to bond with the nuclei and the growing nuclei will coalesce with adjacent ones along the direction perpendicular to the c-axis, decreasing their surface energy and enhancing plate-like nanocrystal formation. This anisotropic behaviour of the Bi_2Te_3 and Sb_2Te_3 nanocrystals is credited to the hexagonal close packed structure (R-3m), which leads to the formation of hexagonal plates. For this reason, purity of phase was a major aim for the products. It is also important to check that amount of EDTA used as larger concentrations of the surfactant could prevent the aggregation of Bi_2Te_3 and Sb_2Te_3 during nucleation. The exact mechanisms for the formation of these nanostructures is still not quite clear.

The ionic reactions which lead to the formation of Bi_2Te_3 nuclei and the subsequent growth to nanoparticles with the redox potentials are given in the following equations. $NaBH_4$ reduces TeO_3^{2-} to Te and the ionic reaction is given in Equation 17 and the half-cell reactions are given by Equations 15 and 16. Equation 18 gives the reaction of the formation of the telluride anions.

$$BH_4^- + 8OH^- \longrightarrow H_2BO_3^- + 5H_2O + 8e^- \quad (-1.24\,V) \quad \text{..... Equation 15}$$

$$TeO_3^{2-} + 3H_2O + 4e^- \longrightarrow Te + 6OH^- \quad (-0.57\,V) \quad \text{..... Equation 16}$$

$$5TeO_3{}^{2-} + 3BH_4{}^{-} + 6OH^{-} + 4e^{-} \longrightarrow 5Te + 3H_2BO_3{}^{-} \quad \text{….. Equation 17}$$

$$Te + 2e^{-} \longrightarrow Te^{2-} \quad (-1.143\,V) \quad \text{….. Equation 18}$$

Equations 19 and 20 show the formation of the bismuth and bismuth cations, respectively. Equation 21 shows the shows the interaction of the EDTA molecules with the bismuth cations. Equation 22 shows the ionic reaction process for the formation of the plate-like anisotropic growth of the Bi_2Te_3 nanocrystals.

$$BiCl_3 + 3e^{-} + 2H^{+} \longrightarrow Bi + Cl^{-} \quad (0.16\,V) \quad \text{….. Equation 19}$$

$$Bi \longrightarrow Bi^{3+} + 3e^{-} \quad (0.308\,V) \quad \text{….. Equation 20}$$

$$Bi^{3+} + EDTA^{2-} \longrightarrow [Bi(EDTA)]^{+} \quad \text{….. Equation 21}$$

One of the pathways for the formation of Bi_2Te_3 nanocrystals from Equations 18 and 21 is given by Equation 22.

$$2[Bi(EDTA)]^{+} + 3Te^{2-} \longrightarrow Bi_2Te_3 + EDTA \quad \text{….. Equation 22}$$

Another pathway for the growth of Bi_2Te_3 nanocrystals is from the direct combination of metallic Bi and Te. Equations 17 and 19 which shows the formation of Bi and Te metals which form the Bi_2Te_3 nanocrystals as given by Equation 23.

$$2Bi + 3Te \longrightarrow Bi_2Te_3 \quad \text{….. Equation 23}$$

For Bi_2Te_3 formation, $E^0{}_{cell} = \big((0.308) + (-1.143)\big) - ((-0.57) + (-1.24) + (0.16))$

$$E^0{}_{cell} = 0.815\,V$$

Since the $E^0{}_{cell} > 0$, the Gibbs free energy $\Delta G^0 < 0$. The negative Gibbs free energy shows that the reaction pathway for the formation of the Bi_2Te_3 nanocrystals is favoured and the reaction can occur spontaneously.

Similar kinetics is seen for the formation of Sb_2Te_3 nanocrystals.

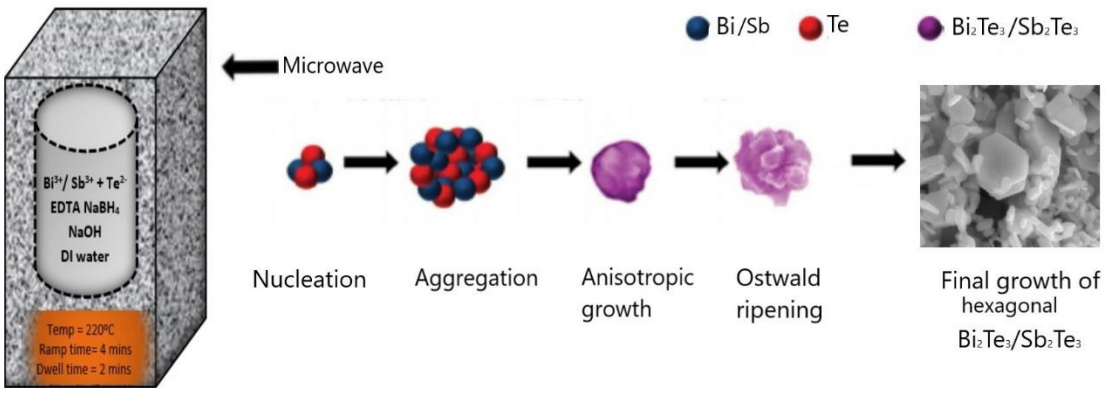

Figure 20. Schematic of the nucleation and growth of Bi_2Te_3 and Sb_2Te_3 hexagonal nanoplates synthesized by microwave assisted aqueous chemical method.

3.3. Particle surface chemistry

Using DLS we have studied the effect of pH on the particles and particle surface chemistry. The colloidal properties of Bi_2Te_3 and Sb_2Te_3 have been studied to analyse the particle size, zeta potential and stability of the particles. When the Bi_2Te_3 and Sb_2Te_3 colloids are introduced to minor changes in pH, the zeta potential show significant variation. Measuring the zeta potential with changing pH is useful in determining the isoelectric point, which helps to study the surface chemistry.

Samples *SW_2a and SW_3* have been analysed by creating a colloidal suspension of the particles. 0.017 gm of the as-synthesized powders was suspended in 200 ml DI water and sonicated. 100 µl of this solution was dispersed in 1ml DI water. The pH is noted for this suspension and Zeta potential size measurements are performed. 5 µl of 0.1 M NaOH is added to increment the change of pH in the alkaline region and similarly, 5 µl of 1 M HCl is added increment the change of pH in the acidic region. Separate couples of samples were used for the acidic and basic titrations and linear increment in pH change was followed to avoid artifacts due to surface reactions during the measurement. Three measurements were carried out for each pH point and the average value has been used to study the surface chemistry. The Zeta potential of Bi_2Te_3 and Sb_2Te_3 as a function of pH of samples *SW_2a and SW_3*, respectively are given in Figures 21 and 22.

From Figures 21 and 22, the isoelectric points for the as-synthesized Bi_2Te_3 and Sb_2Te_3 have been found to pH 6 and 11 respectively. The Zeta potential indicates that at the point of aggregation the colloids are least stable. Apart from the precursors, EDTA is the organic surfactants which could have been present on the surface of the particles. The excessive charge on the surface of the Bi_2Te_3 and Sb_2Te_3 particles as seen from Zeta potential values from Figures 21 and 22 could be due to the EDTA organic molecules.

At regions near the isoelectric point, the particles undergo destabilization, at which the colloids are usually unstable, and the particles tend to coagulate or aggregate. When the particles aggregate as a function of total volume, the surface area increases, and the particle size increases. This study also provides an idea about the stability of the nanoparticles. The more unstable particles are found near the isoelectric points (at Zeta potential ±25 mV) with high particle size, as the particles have aggregated together. The Bi_2Te_3 and Sb_2Te_3 powders are highly charged and seem to be stable at higher pH. The stability of Bi_2Te_3 powder is more than Sb_2Te_3, although they are both largely unstable. This high charge around the particles can be useful for suspending these particles in other medium for the formation of films or for electrophoretic deposition.

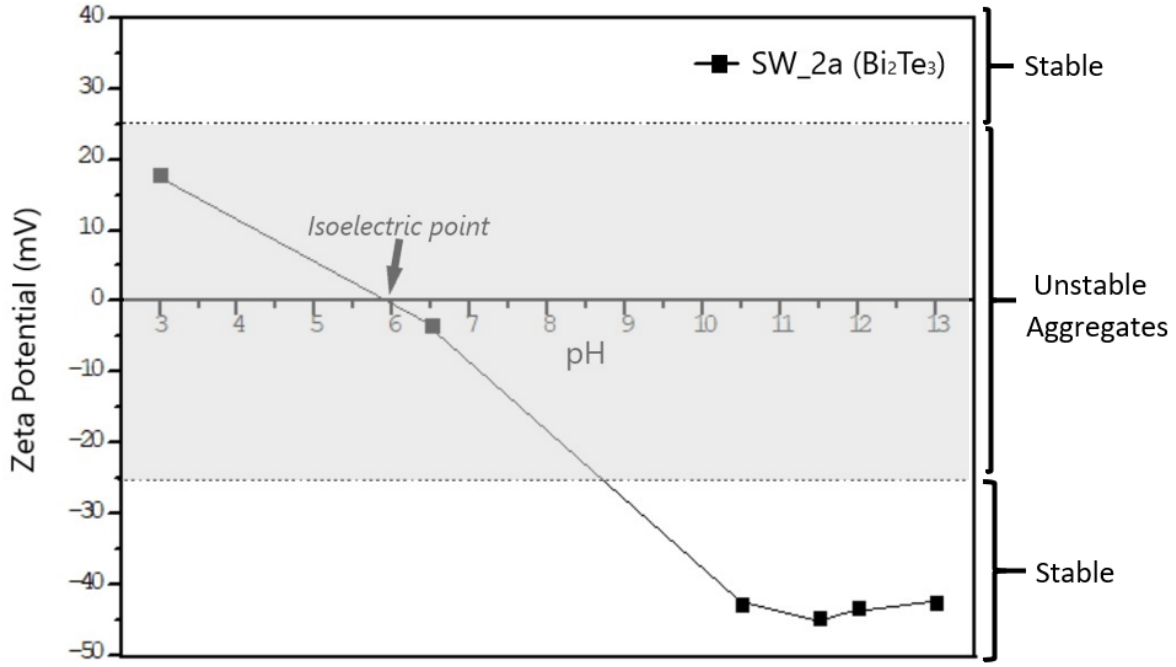

Figure 21. Zeta potential of Bi_2Te_3 as a function of pH.

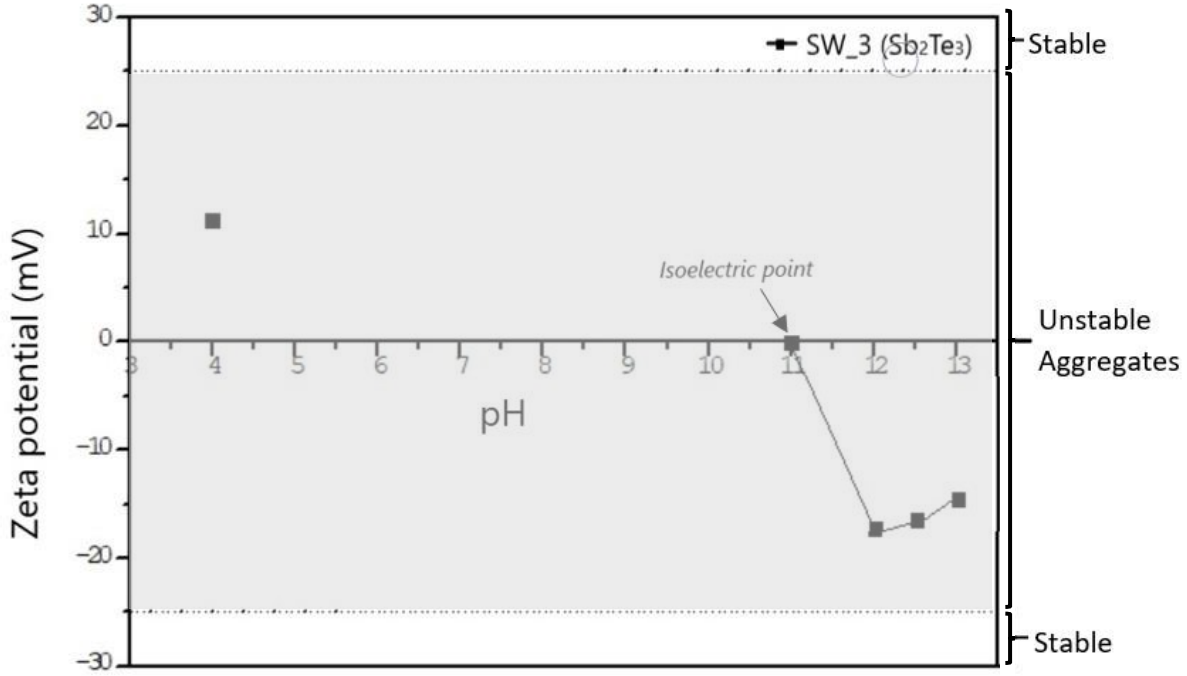

Figure 22. Zeta potential of Sb_2Te_3 as a function of pH.

Chapter 4

Conclusions

In conclusion, good yield of Bi_2Te_3 and Sb_2Te_3 thermoelectric nanomaterials have been successfully prepared by microwave assisted aqueous chemical synthsis method. Thorough optimization of the reaction parameters allowed successful synthesis of highly crystalline, pure and homogeneous Bi_2Te_3 and Sb_2Te_3 hexagonal nanoplates. A simple green and energy efficient method has been developed by utilizing microwave's localized superheating and water as the reaction medium instead of harmful organic solvents for the nucleation of the nanocrystalline Bi_2Te_3 and Sb_2Te_3 TE materials. In order to acknowledge green chemistry, washing with organic chemicals like hexane, methanol was avoided to prevent organic waste in the environment. Compared to the traditional hydrothermal/solvothermal method, this microwave assisted technique provides rapid, high efficiency heating which significantly reduces the reaction time to few minutes instead of hours. Moreover, large volumes can be produced in a single batch with high yield of products. The importance of maintaining a certain pH of the reaction solution is required for the complete reduction of tellurium and for the formation of pure phase structures of Bi_2Te_3 and Sb_2Te_3. Conclusively, an alkaline medium with pH between 10 and 11 has been found to be ideal. The pH also influences the activity of EDTA which is the required for the growth of the particles in the c-axis. The morphology, structure, purity, and crystallinity of the nanoplates have been examined using SEM and XRD, and it can be concluded that these microwave-assisted aqueous chemically produced materials are almost equal to the ones prepared hydrothermally. The size distribution of the Bi_2Te_3 hexagonal nanoplates are 200 nm-1 μm in length and 20-70 nm in thickness and that of Sb_2Te_3 hexagonal nanoplates are 80 nm-1 μm and 30-120 nm in thickness. Few irregular nanoparticles of 30-120 nm diameters are also present. The presence of a mixture of micro and nano structures can play an important role in improving the transport properties. The attempt to scale up the production of the nanocrystals resulted in good yield, but the phase purity and structure can be improved.

Chapter 5

Future Works

Further optimization of the reaction conditions like temperature and time are required to improve the morphology and growth of the nanocrystals. Characterization tools like X-ray photoelectron spectroscopy (XPS), Energy dispersive x-ray spectroscopy (EDS or EDX), Fourier-transform infrared spectroscopy (FTIR) and Transmission electron microscopy (TEM) are required to understand the properties and nature of the Bi_2Te_3 and Sb_2Te_3 nanoplates. Spark plasma sintering (SPS) will be done to make consolidated compact powders. We then plan to make thin films from these sintered powders and measure the figure of merit. We would also like to prepare large volumes of the prepared Bi_2Te_3 and Sb_2Te_3 samples taking benefits of the microwave heating.

Bibliography

[1] Over Shoot Day 2019, Global Footprint Network (July 2019) footprintnetwork.org/2019/07/23/press-release-july-2019/

[2] Royal Institution of Great Britain, rigb.org/docs/faraday_notebooks_colloids_0.pdf

[3] Faraday, M.. *X. The Bakerian Lecture. — Experimental relations of gold (and other metals) to light*, Phil. Trans. R. Soc. **147** doi: 10.1098/rstl.1857.0011

[4] Long, N. N., Vu, L. V., Kiem, C. D., Doanh, S. C., Nguyet, C. T., *et al.* (2009) *Synthesis and optical properties of colloidal gold nanoparticles*. J. Phys. Conf. Ser. **187**, 012026. doi:10.1088/1742-6596/187/1/012026

[5] Feynman, R. P. (1960) *There's Plenty of Room at the Bottom.* Engineering and Science, 23, 5, 22-36. ISSN 0013-7812

[6] Scientific Committee on Emerging and Newly Identified Health Risks (SCENIHR) (March 2006), SCENIHR /002/05, *The appropriateness of existing methodologies to assess the potential risks associated with engineered and adventitious products of nanotechnologies*.

[7] Cao, G. (2004) *Nanostructures and Nanomaterials. Synthesis, Properties, and Applications*. Imperial College Press, London. ISBN 1-86094-4159

[8] Pradeep, T. (2007) *NANO: The Essentials: Understanding Nanoscience and Nanotechnology*, Tata McGraw-Hill Publishing Company Limited. doi: 10.1036/0071548297

[9] Edvinsson, T. (2018). *Optical quantum confinement and photocatalytic properties in two-, one- and zero-dimensional nanostructures*. Royal Society Open Science, **5**, 9, 180387. doi:10.1098/rsos.180387

[10] Hu, C. (2010) *Modern Semiconductor Devices for Integrated Circuits*. Upper Saddle River, N.J. Prentice Hall.

[11] Linkov, I., and Steevens, J. (2009). *Nanomaterials: Risks and Benefits*, Springer. doi: 10.1007/978-1-4020-9491-0

[12] Vaseashta, A., Riesfeld, R., and Mihailescu, I. N. (2008) *Green Nanotechnologies for Responsible Manufacturing* in The Business of Nanotechnology, edited by Gandhi, A., Giordani, S., Merhari, L., Tsakalakos, L., and Tsamis, C., in Materials Research Society Spring meeting. Proc. 1106E, #1106-PP03-05. Warrendale, PA.

[13] Anastas, P., and Eghbali, N. (2010). *Green Chemistry: Principles and Practice.* Chem. Soc. Rev., **39**(1), 301–312. doi:10.1039/b918763b

[14] *Environment and Green Nano, Green Nanotechnology I—What Is It* 2006, nanotechproject.org/events/archive/green_nanotechnology_iwhat_it/

[15] Palmén, C. *Waste heat is everywhere – Let's put it in use*, June 4 2019, climeon.com/waste-heat-is-everywhere-lets-put-it-in-use/

[16] Jouhara, H., Khordehgah, N., Almahmoud, S., Delpech, B., Chauhan, A., and Tassou, S. A. (2018). *Waste heat recovery technologies and applications.* Thermal Science and Engineering Progress, **6**, 268–289. doi: 10.1016/j.tsep.2018.04.017

[17] Moore, G. E. (1998) *Cramming more components onto integrated circuits,* Proceedings of the IEEE, Vol. 86, 82 – 85. doi: 10.1109/JPROC.1998.658762

[18] Shockley, W. (1949). *The theory of p-n junctions in semiconductors and p-n junction transistors.* The Bell System Technical Journal, **28**(3), 435–489. doi:10.1002/j.1538-7305.1949. tb03645.x.

[19] Petsagkourakis, I., Tybrandt, K., Crispin, X., Ohkubo, I., Satoh, N., and Mori, T. (2018). *Thermoelectric materials and applications for energy harvesting power generation.* Science and Technology of Advanced Materials, **19**, 1, 836–862. doi:10.1080/14686996.2018.1530938

[20] Sajid, M., Hassan, I., and Rahman, A. (2017). *An overview of cooling of thermoelectric devices*. Renewable and Sustainable Energy Reviews, **78**, 15–22. doi: 10.1016/j.rser.2017.04.098

[21] Fitriani, Ovik, R., Long, B. D., Barma, M. C., Riaz, M., Sabri, M. F. M., Saidur, R. (2016). *A review on nanostructures of high-temperature thermoelectric materials for waste heat recovery*. Renewable and Sustainable Energy Reviews**, 64**, 635–659. doi: 10.1016/j.rser.2016.06.035

[22] Huen, P., and Daoud, W., A. (2017). *Advances in hybrid solar photovoltaic and thermoelectric generators*. Renewable and Sustainable Energy Reviews, **72**, 1295–1302. doi: 10.1016/j.rser.2016.10.042

[23] Champier D. (2017). *Thermoelectric generators: a review of applications*. Energy Conversion and Management, **140**, 167–81. doi: 10.1016/j.enconman.2017.02.070 0196-8904.

[24] Snyder, G. J. and Toberer, E. S. (2008). *Complex thermoelectric materials.* Nature Materials, **7**(2), 105–114. doi:10.1038/nmat2090

[25] Maciá, E. (2015) *Thermoelectric Materials: Fundamentals and Applications,* Pan Stanford Publishing, 2015. ISBN-13: 978-981-4463-53-9

[26] Seebeck, T. J. (1826). *Ueber die magnetische Polarisation der Metalle und Erze durch Temperaturdifferenz*. Annalen Der Physik, **82(**3), 253–286. doi:10.1002/andp.18260820302

[27] Hofmann, A. I., Kroon, R. and Müller, C. (2019). *Doping and processing of organic semiconductors for plastic thermoelectrics*. Handbook of Organic Materials for Electronic and Photonic Devices, 429–449. doi: 10.1016/b978-0-08-102284-9.00013-9

[28] Bubnova, O., Khan, Z. U., Wang, H., Braun, S., Evans, D. R., Fabretto, M., Talemi, P. H. *et al.* (2013). *Semi-metallic polymers*. Nature Materials, **13**(2), 190–194. doi: 10.1038/nmat3824

[29] Peltier, J. (1834). *Nouvelles expériences sur la caloricité des courants électrique (New experiments on the heat effects of electric currents),* Annales de Chimie et de Physique, **56**, 371-386.

[30] Lenz, E. (1838). *Einige Versuche im Gebiete des Galvanismus. Annalen Der Physik Und Chemie*, 120(6), 342–349. doi:10.1002/andp.18381200612

[31] Thomson, W. (1851), *On a mechanical theory of thermo-electric currents*. Proceedings of the Royal Society of Edinburgh. **3,** 42, 91–98

[32] Yatsyshyn, S., Stadnyk B., Lutsyk, Y., Buniak, L. *Handbook of Thermometry and Nanothermometry*, International Frequency Sensor Association (IFSA) Publishing, Spain, (2015), ISBN: 978-84-606-7518-1, e-ISBN: 978-84-606-7852-6

[33] Ioffe, A. F. (1957), *Semiconductor Thermoelements and Thermoelectric Cooling*, Infosearch Ltd., London

[34] Kittel, C. (2004), *Introduction to Solid State Physics*, Wiley, 8th edition, ISBN: 978-0-471-41526-8

[35] Altenkirch, E. (1909). *Uber den Nortzeffkt der Thermosaule. Physikalische Zeitschrift*, **10**, 560–580

[36] Llin, L. F., Paul, D. J., *9. Thermoelectrics, Photovoltaics and Thermal Photovoltaics for Powering ICT Devices and Systems Book* - ICT - Energy Concepts for Energy Efficiency and Sustainability. InTechOpen (2017) ISBN: 978-953-51-3012-3, eBook (PDF) ISBN: 978-953-51-4894-4, doi: 10.5772/65983

[37] Snyder, G. J., and Snyder, A. H. (2017). *Figure of merit ZT of a thermoelectric device defined from materials properties*. Energy & Environmental Science, **10(**11), 2280–2283. doi:10.1039/c7ee02007d

[38] Szczech, J. R., Higgins, J. M., and Jin, S. (2011). *Enhancement of the thermoelectric properties in nanoscale and nanostructured materials.* Journal of Materials Chemistry, **21**(12), 4037–4055. doi: 10.1039/c0jm02755c

[39] Kim, H. S., Liu, W., Chen, G., Chu, C. W., and Ren, Z. (2015). *Relationship between thermoelectric figure of merit and energy conversion efficiency*. Proceedings of the National Academy of Sciences, **112**(27), 8205–8210. doi: 10.1073/pnas.1510231112

[40] Wood, C. (1988). Materials for thermoelectric energy conversion. Reports on Progress in Physics, **51**(4), 459–539. doi:10.1088/0034-4885/51/4/001

[41] Masood, K. B., Kumar, P., Singh, R. A., and Singh, J. (2018). *Odyssey of thermoelectric materials: foundation of the complex structure*. Journal of Physics Communications, **2**(6), 062001. doi: 10.1088/2399-6528/aab64f

[42] Rowe, D. M., Shukla, V. S., and Savvides, N. (1981). *Phonon scattering at grain boundaries in heavily doped fine-grained silicon–germanium alloys.* Nature, **290(**5809), 765–766. doi: 10.1038/290765a0

[43] Hicks, L. D., and Dresselhaus, M. S. (1993). *Effect of quantum-well structures on the thermoelectric figure of merit*. Physical Review B, **47**(19), 12727–12731. doi: 10.1103/physrevb.47.12727

[44] Hicks, L. D., and Dresselhaus, M. S. (1993). *Thermoelectric figure of merit of a one-dimensional conductor*. Physical Review B, **47**(24), 16631–16634. doi: 10.1103/physrevb.47.16631

[45] Venkatasubramanian, R., Siivola, E., Colpitts, T., and O'Quinn, B. (2001). *Thin-film thermoelectric devices with high room-temperature figures of merit.* Nature, **413**(6856), 597–602. doi: 10.1038/35098012

[46] Novak, T. G., Kim, K., and Jeon, S. (2019). *2D and 3D Nanostructuring Strategies for Thermoelectric Materials.* Nanoscale, **11**, 19684-19699 doi: 10.1039/c9nr07406f

[47] Zhao, X. B., Ji, X. H., Zhang, Y. H., Zhu, T. J., Tu, J. P., and Zhang, X. B. (2005). *Bismuth telluride nanotubes and the effects on the thermoelectric properties of nanotube-containing nanocomposites.* Applied Physics Letters, **86**(6), 062111. doi: 10.1063/1.1863440

[48] Wang, Z., Wang, F., Chen, H., Zhu, L., Yu, H., and Jian, X. (2010). *Synthesis and characterization of Bi_2Te_3 nanotubes by a hydrothermal method.* Journal of Alloys and Compounds, **492**(1-2), L50–L53. doi: 10.1016/j.jallcom.2009.11.155

[49] Forman, C., Muritala, I. K., Pardemann, R., and Meyer, B. (2016). *Estimating the global waste heat potential*. Renewable and Sustainable Energy Reviews, **57**, 1568–1579. doi: 10.1016/j.rser.2015.12.192

[50] Foos, E. E., Stroud, R. M., and Berry, A. D. (2001). *Synthesis and Characterization of Nanocrystalline Bismuth Telluride.* Nano Letters, **1**(12), 693–695. doi: 10.1021/nl0156179

[51] Kim, H. J., Han, M. K, Kim, H. Y., Lee, W., and Kim, S. J. (2012). *Morphology Controlled Synthesis of Nanostructured Bi_2Te_3.* Bulletin of the Korean Chemical Society, **33**(12), 3977–3980. doi: 10.5012/BKCS.2012.33.12.3977

[52] AZO Materials azom.com/article.aspx?ArticleID=8462

[53] Kim, C., Kim, D. H., Han, Y. S., Chung, J. S., and Kim, H. (2011). *Fabrication of antimony telluride nanoparticles using a brief chemical synthetic process under atmospheric conditions*. Journal of Alloys and Compounds, **509**(3), 609–613. doi: 10.1016/j.jallcom.2010.10.002

[54] AZO Materials azom.com/article.aspx?ArticleID=2281

[55] Son, J. H., Oh, M. W., Kim, B. S., Park, S. D., Min, B. K., Kim, M. H., and Lee, H. W. (2013). *Effect of ball milling time on the thermoelectric properties of p-type $(Bi,Sb)_2Te_3$.* Journal of Alloys and Compounds, **566**, 168–174. doi: 10.1016/j.jallcom.2013.03.062

[56] Gahtori, B., Bathula, S., Tyagi, K., Jayasimhadri, M., Srivastava, A. K., Singh, S., Dhar, A. (2015). *Giant enhancement in thermoelectric performance of copper selenide by incorporation of different nanoscale dimensional defect features.* Nano Energy, **13**, 36-46. doi: 10.1016/j.nanoen.2015.02.008

[57] Raihan, O., Mohd Said, S., Sabri, M. F. M., Rozali, S., Long, B. D., Kimura, K., Tobita, K., Fitriani, Salleh, M. F. M., Ali Bashir, M. B. (2018). *Parametric analysis of ball milling condition on thermoelectric performance of $Bi_{0.6}FeCo_3Sb_{12}$ skutterudite*. Materials Research Express, **5**(19) 105008. ISSN 2053-1591. doi: 10.1088/2053-1591/aada92

[58] Zheng, Y., Liu, C., Miao, L., Lin, H., Gao, J., Wang, X., Chen, J., Wu, S., Li, X., Cai, H. (2018). *Cost effective synthesis of p-type Zn-doped MgAgSb by planetary ball-milling with enhanced thermoelectric properties.* RSC Advances, **8**(62), 35353–*35359*. doi: 10.1039/c8ra06765a

[59] Giani, A., Pascal-Delannoy, F., Boyer, A., Foucaran, A., Gschwind, M., and Ancey, P. (1997). *Elaboration of Bi_2Te_3 by metal organic chemical vapor deposition.* Thin Solid Films, **303**(1-2), 1–3. doi:10.1016/s0040-6090(97)00089-8

[60] Venkatasubramanian, R., Colpitts, T., Watko, E., Lamvik, M., and El-Masry, N. (1997). *MOCVD of Bi_2Te_3, Sb_2Te_3 and their superlattice structures for thin-film thermoelectric applications.* Journal of Crystal Growth, **170**(1-4), 817–821. doi:10.1016/s0022-0248(96)00656-2

[61] Longo, M., Cecchi, S., Selmo, S., Fanciulli, M., Wiemer, C., Battaglia, J. L., Saci, A., Kusiak, A. (2015). *MOCVD growth and thermal analysis of Sb_2Te_3 thin films and nanowires*. 2015 1st Workshop on Nanotechnology in Instrumentation and Measurement (NANOFIM). doi: 10.1109/nanofim.2015.8425350

[62] Lee, J. S., Brittman, S., Yu, D., and Park, H. (2008). *Vapor–Liquid–Solid and Vapor–Solid Growth of Phase-Change Sb_2Te_3 Nanowires and Sb_2Te_3 /GeTe Nanowire Heterostructures*. Journal of the American Chemical Society, **130**(19), 6252–6258. doi: 10.1021/ja711481b

[63] Park, D., Park, S., Jeong, K., Jeong, H. S., Song, J. Y., and Cho, M. (2016). *Thermal and Electrical Conduction of Single-crystal Bi_2Te_3 Nanostructures grown using a one step process*. Scientific Reports, **6**(1). doi: 10.1038/srep19132

[64] Gupta, S., Neeleshwar, S., Kumar, V., Chen, Y.Y., (2012). *Synthesis of bismuth telluride nanostructures by refluxing method.* Advanced Materials Letters, **3**(1), 50-54. doi: 10.5185/amlett.2011.7285

[65] Pelz, U., Kaspar, K., Schmidt, S., Dold, M., Jägle, M., Pfaadt, A., and Hillebrecht, H. (2012). *An Aqueous-Chemistry Approach to Nano-Bismuth Telluride and Nano-Antimony Telluride as Thermoelectric Materials.* Journal of Electronic Materials, **41**(6), 1851–1857. doi: 10.1007/s11664-012-2099-1

[66] Yang, H. Q., Miao, L., Liu, C. Y., Li, C., Honda, S., Iwamoto, Y., Huang, R., Tanemura, S. (2015). *A Facile Surfactant-Assisted Reflux Method for the Synthesis of Single-Crystalline Sb_2Te_3 Nanostructures with Enhanced Thermoelectric Performance.* ACS Applied Materials & Interfaces, **7**(26), 14263–14271. doi: 10.1021/acsami.5b02504

[67] Sapp, S. A., Lakshmi, B. B., and Martin, C., R. (1999). *Template Synthesis of Bismuth Telluride Nanowires.* Advanced Materials, **11**(5), 402–404. doi: 10.1002/(sici)1521-4095(199903)11:5<402::aid-adma402>3.0.co;2-l

[68] Pinisetty, D., Gupta, M., Karki, A. B., Young, D. P., and Devireddy, R. V. (2011). *Fabrication and characterization of electrodeposited antimony telluride crystalline nanowires and nanotubes*. Journal of Materials Chemistry, **21**(12), 4098–4107. doi: 10.1039/c0jm01969k

[69] Dhak, D., and Pramanik, P. (2006). *Characterization of Nanocrystalline Bismuth Telluride (Bi_2Te_3) Synthesized by a Novel Approach Through Aqueous Precursor Method*. Journal of the American Ceramic Society, **89**(2), 534–537. doi: 10.1111/j.1551-2916.2005.00784.x

[70] Saleemi, M., Toprak, M. S., Li, S., Johnsson, M., and Muhammed, M. (2012). *Synthesis, processing, and thermoelectric properties of bulk nanostructured bismuth telluride (Bi_2Te_3).* Journal of Materials Chemistry, **22(**2), 725–730. doi: 10.1039/c1jm13880d

[71] Zhao, X., Ji, X., Zhang, Y., and Lu, B. (2004). *Effect of solvent on the microstructures of nanostructured Bi_2Te_3 prepared by solvothermal synthesis.* Journal of Alloys and Compounds, **368**(1-2), 349–352. doi: 10.1016/j.jallcom.2003.08.070

[72] Deng, Y., Zhou, X., Wei, G., Liu, J., Nan, C.W., and Zhao, S. (2002). *Solvothermal preparation and characterization of nanocrystalline Bi_2Te_3 powder with different morphology.* Journal of Physics and Chemistry of Solids, **63**(11), 2119–2121. doi: 10.1016/s0022-3697(02)00261-5

[73] Deng, Y., Nan, C. W., Wei, G. D., Guo, L., and Lin, Y. (2003). *Organic-assisted growth of bismuth telluride nanocrystals.* Chemical Physics Letters, **374**(3-4), 410–415. doi: 10.1016/s0009-2614(03)00783-8

[74] Jin, R., Liu, J., and Li, G. (2014). *Facile solvothermal synthesis, growth mechanism and thermoelectric property of flower-like Bi_2Te_3.* Crystal Research and Technology, **49**(7), 460–466. doi: 10.1002/crat.201400012

[75] Stavila, V., Robinson, D. B., Hekmaty, M. A., Nishimoto, R., Medlin, D. L., Zhu, S., Tritt T.M, Sharma, P. A. (2013). *Wet-Chemical Synthesis and Consolidation of Stoichiometric Bismuth Telluride Nanoparticles for Improving the Thermoelectric Figure-of-Merit.* ACS Applied Materials & Interfaces, **5**(14), 6678–6686. doi: 10.1021/am401444w

[76] Xu, Y., Ren, Z., Cao, G., Ren, W., Deng, K., and Zhong, Y. (2009). *Fabrication and characterization of Bi_2Te_3 nanoplates via a simple solvothermal process.* Physica B: Condensed Matter, **404**(21), 4029–4033. doi: 10.1016/j.physb.2009.07.153

[77] Sun, S., Peng, J., Jin, R., Song, S., Zhu, P., and Xing, Y. (2013). *Template-free solvothermal synthesis and enhanced thermoelectric performance of Sb_2Te_3 nanosheets*. Journal of Alloys and Compounds, **558**, 6–10. doi: 10.1016/j.jallcom.2013.01.017

[78] Im, H. J., Koo, B., Kim, M. S., and Lee, J. E. (2019). *Solvothermal synthesis of Sb_2Te_3 nanoplates under various synthetic conditions and their thermoelectric properties*. Applied Surface Science, **475**, 510–514. doi: 10.1016/j.apsusc.2019.01.014

[70] Wang, P. B., Yang, J., Wang, D. Z., and Ren, Z. F. (2005). *High-Yield Synthesis of Single-Crystalline Antimony Telluride Hexagonal Nanoplates Using a Solvothermal Approach*. Journal of the American Chemical Society, **127**(40), 13792–13793. doi: 10.1021/ja054861p

[80] Kim, C., Kim, D. H., Han, Y. S., Chung, J. S., Park, S., and Kim, H. (2011). *Fabrication of bismuth telluride nanoparticles using a chemical synthetic process and their thermoelectric evaluations.* Powder Technology, **214(**3), 463–468. doi: 10.1016/j.powtec.2011.08.049

[81] Giri, L., Mallick, G., Jackson, A. C., Griep, M. H., and Karna, S. P. (2015). *Synthesis and characterization of high-purity, single phase hexagonal Bi_2Te_3 nanostructures*. RSC Advances, **5**(32), 24930–24935. doi: 10.1039/c5ra02303c

[82] Xu, Y., Ren, Z., Ren, W., Cao, G., Deng, K., and Zhong, Y. (2008). *Hydrothermal synthesis of single-crystalline Bi_2Te_3 nanoplates.* Materials Letters, **62**(27), 4273-4276. doi: 10.1016/j.matlet.2008.06.055

[83] Sun, T., Zhao, X. B., Zhu, T. J., and Tu, J. P. (2006). *Aqueous chemical reduction synthesis of Bi_2Te_3 nanowires with surfactant assistance*. Materials Letters, **60**(20), 2534–2537. doi: 10.1016/j.matlet.2006.01.033

[84] Cao, Y. Q., Zhu, T. J., and Zhao, X. B. (2008). *Thermoelectric Bi_2Te_3 nanotubes synthesized by low-temperature aqueous chemical method.* Journal of Alloys and Compounds, **449**(1-2), 109–112. doi: 10.1016/j.jallcom.2006.01.116

[85] Shi, W., Yu, J., Wang, H., and Zhang, H. (2006). *Hydrothermal Synthesis of Single-Crystalline Antimony Telluride Nanobelts*. Journal of the American Chemical Society, **128**(51), 16490–16491. doi: 10.1021/ja066944r

[86] Dong, G. H., Zhu, Y. J., Cheng, G. F., and Ruan, Y.J. (2013). *Sb_2Te_3 nanobelts and nanosheets: Hydrothermal synthesis, morphology evolution and thermoelectric properties*. Journal of Alloys and Compounds, **550**, 164–168. doi: 10.1016/j.jallcom.2012.09.061

[87] Yuan, Q., Nie, Q., and Huo, D. (2009). *Preparation and characterization of the antimony telluride hexagonal nanoplates*. Current Applied Physics, **9**(1), 224–226. doi:10.1016/j.cap.2008.01.015

[88] Dharmaiah, P., and Hong, S. J. (2017). *Hydrothermal method for the synthesis of Sb_2Te_3, and $Bi_{0.5}Sb_{1.5}Te_3$ nanoplates and their thermoelectric properties.* International Journal of Applied Ceramic Technology, **15**(1), 132–139. doi: 10.1111/ijac.12762

[89] Novaconi, S., Vlazan, P., Malaescu, I., Badea, I., Grozescu, I., and Sfirloaga, P. (2013). *Doped Bi_2Te_3 nano-structured semiconductors obtained by ultrasonically assisted hydrothermal method.* Open Chemistry, **11**(10). doi: 10.2478/s11532-013-0291-7

[90] Zheng, Y. Y., Zhu, T. J., Zhao, X. B., Tu, J. P., and Cao, G. S. (2005). *Sonochemical synthesis of nanocrystalline Bi_2Te_3 thermoelectric compounds*. Materials Letters, **59**(23), 2886–2888. doi: 10.1016/j.matlet.2005.04.035

[91] Zhou, B., Zhao, Y., Pu, L., and Zhu, J. J. (2006). *Microwave-assisted synthesis of nanocrystalline Bi_2Te_3. Materials Chemistry and Physics,* **96**(2-3), 192–196. doi: 10.1016/j.matchemphys.2005.07.010

[92] Dong, G. H., Zhu, Y. J., and Chen, L. D. (2010). *Microwave-assisted rapid synthesis of Sb_2Te_3 nanosheets and thermoelectric properties of bulk samples prepared by spark plasma sintering*. Journal of Materials Chemistry, **20**(10), 1976. doi: 10.1039/b915107a

[93] Zhang, Y., Xu, G., Mi, J., Han, F., Wang, Z., and Ge, C. (2011). *Hydrothermal synthesis and thermoelectric properties of nanostructured $Bi_{0.5}Sb_{1.5}Te_3$ compounds.* Materials Research Bulletin, **46**(5), 760–764. doi: 10.1016/j.materresbull.2010.11.024

[94] Cravotto, G., and Carnaroglio, D. (2017). *Microwave Chemistry*. Berlin, Boston: De Gruyter. ISBN: 978-3-11-047993-5

[95] Nadagouda, M. N., Speth, T. F., and Varma, R. S. (2011). *Microwave-Assisted Green Synthesis of Silver Nanostructures.* Accounts of Chemical Research, **44**(7), 469–478. doi:10.1021/ar1001457

[96] Gou, L., Chipara, M., and Zaleski, J. M. (2007). *Convenient, Rapid Synthesis of Ag Nanowires.* Chemistry of Materials, **19**(7), 1755–1760. doi: 10.1021/cm070160a

[97] Köseoglu, Y., Yıldız, H., and Yilgin, R. (2012). *Synthesis, Characterization and Superparamagnetic Resonance Studies of $ZnFe_2O_4$ Nanoparticles*. Journal of Nanoscience and Nanotechnology, **12**(3), 2261–2269. doi: 10.1166/jnn.2012.5718

[98] Pires, F. I., Joanni, E., Savu, R., Zaghete, M. A., Longo, E., and Varela, J. A. (2008). *Microwave-assisted hydrothermal synthesis of nanocrystalline SnO powders.* Materials Letters, **62**(2), 239–242. doi: 10.1016/j.matlet.2007.05.006

[99] Gao, F., Lu, Q., and Komarneni, S. (2005). *Interface Reaction for the Self-Assembly of Silver Nanocrystals under Microwave-Assisted Solvothermal Conditions*. Chemistry of Materials, **17**(4), 856–860. doi: 10.1021/cm048663t

[100] Kasapoglu, N., Baykal, A., Koseoglu, Y., and Toprak, M. (2007). *Microwave-assisted combustion synthesis of $CoFe_2O_4$ with urea, and its magnetic characterization.* Scripta Materialia, **57**(5), 441–444. doi: 10.1016/j.scriptamat.2007.04.042

[101] Nehru, L. C., Swaminathan, V., and Sanjeeviraja, C. (2012). *Rapid synthesis of nanocrystalline ZnO by a microwave-assisted combustion method.* Powder Technology, **226**, 29–33. doi: 10.1016/j.powtec.2012.03.042

[102] Liao, X. H., Chen, N. Y., Xu, S., Yang, S. B., and Zhu, J. J. (2003). *A microwave assisted heating method for the preparation of copper sulfide nanorods.* Journal of Crystal Growth, **252**(4), 593–598. doi: 10.1016/s0022-0248(03)01030-3

[103] Zito, C. A., Orlandi, M. O., and Volanti, D. P. (2018). *Accelerated microwave-assisted hydrothermal/solvothermal processing: Fundamentals, morphologies, and applications.* Journal of Electroceramics, **40**(4), 271–292

[104] Kolhatkar, G., Vargas, F. A., Thomas, R., and Ruediger, A. (2017). *Microwave-Assisted Hydrothermal Synthesis of $BiFe_xCr_{1-x}O_3$ Ferroelectric Thin Films*. Crystal Growth & Design, **17**(11), 5697–5703. doi: 10.1021/acs.cgd.7b00603

[105] Qiu, G., Dharmarathna, S., Zhang, Y., Opembe, N., Huang, H., and Suib, S. L. (2011*). Facile Microwave-Assisted Hydrothermal Synthesis of CuO Nanomaterials and Their Catalytic and Electrochemical Properties.* Journal of Physical Chemistry C, **116**(1), 468–477.doi: 10.1021/jp209911k

[106] Nehru, L. C., and Sanjeeviraja, C. (2014). *Rapid synthesis of nanocrystalline SnO_2 by a microwave-assisted combustion method*. Journal of Advanced Ceramics, **3**(3), 171–176. doi: 10.1007/s40145-014-0101-5

[107] Qiu, G., Dharmarathna, S., Genuino, H., Zhang, Y., Huang, H., and Suib, S. L. (2011). *Facile Microwave-Refluxing Synthesis and Catalytic Properties of Vanadium Pentoxide Nanomaterials*. ACS Catalysis, **1**(12), 1702–1709. doi: 10.1021/cs200437x

[108] Zeynizadeh, B., and Setamdideh, D. (2005). *Water as a Green Solvent for Fast and Efficient Reduction of Carbonyl Compounds with $NaBH_4$ under Microwave Irradiation*. Journal of the Chinese Chemical Society, **52**(6), 1179–1184. doi: 10.1002/jccs.200500169

[109] Akerlof, G. C., and Oshry, H. I. (1950). *The Dielectric Constant of Water at High Temperatures and in Equilibrium with its Vapor.* Journal of the American Chemical Society, **72**(7), 2844–2847. doi: 10.1021/ja01163a006

TRITA -SCI-GRU 2020:009